Electrospun Hollow Nanofiber Surfaces as Dielectric Mediums for Highly Sensitive Flexible Capacitive Pressure Sensors in Low pressure Regimes

Department of Mechanical and Materials Engineering, Turku University

Master`s thesis

Author:
Shaharyar Siddique

28.06.2025

Turku

Master's thesis
Subject: MSc. in Materials Engineering Technology (Modern Industrial Materials Track)
Author: Shaharyar Siddique
Title: Electrospun Hollow Nanofiber Surfaces as Dielectric Mediums for Highly Sensitive Flexible Capacitive Pressure Sensors in Low pressure Regimes
Supervisors: Doctoral Researcher, Amit Barua, Assistant Professor, Vipul Sharma
Number of pages: 79 pages
Date: 28.06.2025

Abstract

Flexible capacitive pressure sensors have gained importance in the electronics industry with varying structural designs for monitoring, soft robotics and sensing needs. However, achieving high sensitivity at low-pressures with soft, flexible, and scalable dielectric materials remains a key challenge. It requires dielectric layers that are both soft and low permittivity to achieve high sensitivity. This thesis addresses this challenge by developing a flexible capacitive pressure sensor that employs coaxially electrospun hollow polycaprolactone (PCL) nanofibers as a compressible dielectric spacer. The process produces continuous core–shell fibers with a removable inner core, yielding thin-walled hollow fibers with enhanced air-gap volume. Compared to conventional solid nanofiber dielectrics, the hollow fiber dielectric exhibits significantly higher sensitivity in the low-pressure regime due to increased compressibility and a lower effective permittivity. The sensor achieved a maximum sensitivity of approximately 1.05 kPa^{-1} at low-pressure, while also demonstrating good cyclic stability and a fast response. These results indicate that the coaxial electrospinning approach is highly scalable, and integration with 3D printing as well as dielectric property enhancements are proposed to further advance its performance.

Keywords: Capacitive Pressure Sensors, Coaxial Electrospinning, Polycaprolactone PCL, Dielectric, Sensitivity.

Acknowledgement

I would like to express my sincere gratitude to the Materials for Flexible Devices group at the University of Turku for the opportunity to work on this research project. I am especially thankful to Dr. Vipul Sharma for his guidance and mentorship throughout the process. I would also like to thank my group members Amit Barua and Dr. Rituporn Gogoi for their continuous support, insightful discussions, and collaboration spirit during the development of this thesis and the successful publication of our article in the IEEE Journal on Flexible Electronics. In addition, I also gratefully acknowledge Dr. Ermei Mäkilä for his kind assistance in preparing the samples for cross-sectional analysis which was crucial in providing the proof of concept.

I am deeply grateful to my family for their unwavering emotional support, love and encouragement throughout this journey. Their belief in me has been a constant source of strength and motivation especially during challenging times.

Finally, I would like to thank all those who, directly or indirectly, contributed to this work and made this journey a memorable and meaningful one.

Table of contents

Table of Figures

List of Tables

List of Abbreviations and Symbols

PCL	Polycaprolactone
ITO	Indium Tin Oxide
PET	Polyethylene terephthalate
PVA	Polyvinyl alcohol
SEM	Scanning Electron Microscopy
TCD	Tip-to-Collector Distance
PDMS	Polydimethylsiloxane
PU	Polyurethane
CNT	Carbon Nanotubes
BT	Barium Titanate
TPU	Thermoplastic Polyurethane Urethane
AgNWs	Silver Nanowires
PVDF	Polyvinylidene fluoride
PI	Polyimide
CuNWs	Copper Nanowires
SCA	Strontium Alginate
C	Capacitance (F)
ΔC	Change in capacitance (F)
C_o	Baseline capacitance (F)
ΔP	Change in pressure (Pa or kPa)
ε_0	Vacuum permittivity (8.854×10^{-12} Fm^{-1})

ε_r	Relative permittivity (dimensionless)
A	Electrode overlap area (m^2)
d	Distance between electrodes (m)
d_{in}	Inner core thickness (m)
d_{shell}	Polymer nanofiber wall thickness (m)
d_{out}	Outer dielectric thickness (m)
V	Voltage (V)
R	Resistance (Ω)
I	Current (A)
σ	Electrical conductivity (Sm^{-1})
ε	Permittivity (general)

1 Introduction

In recent years, the evolution of flexible electronics has enhanced the development of advanced sensing technologies for human centred applications. This has made the development of highly sensitive capacitive pressure sensors inevitable. These sensors mimic the sensory functions of human skin, making them integral to electronic skin used in prosthetics, robotics and soft interfaces [1][2][3]. It facilitates non-invasive tracking of physiological signals such as pulse, respiration and body movement. Capacitive pressure sensors operate on the principle of a parallel plate capacitor. Once pressure is applied, the capacitance changes due to the mechanical deformation between the plates. In such designs, changes in the microstructure of the dielectric layer under pressure also contribute to the change in capacitance [4]. The relative change in capacitance per unit pressure determines the sensitivity of the sensor.

The sensitivity of the sensors depends on several factors i.e., dielectric material, conductive surfaces and the spacing between the conductive surfaces. Although flexible capacitive sensors have a simple structure, mechanical flexibility and low power requirement but they have certain limitations as well. The prominent challenge is their ability to sense at very low-pressures. Most traditional dielectrics are made from planar surfaces and hence show limited compressibility at low-pressure. Consequently, the change in the area between the plates varies very little, showing quite less sensitivity. In addition, flat surfaces lack structural features e.g., air gaps, hollow channels etc. that would enhance pressure-induced deformation [5]. Traditional pressure sensors show a non-linear response either in the low-pressure regime or in saturation at high-pressures. This has led to the development of nanostructured dielectric layers having porosity and hollow channels to be more responsive to low-pressures as shown in Figure 1(a), (b) and (c) [6].

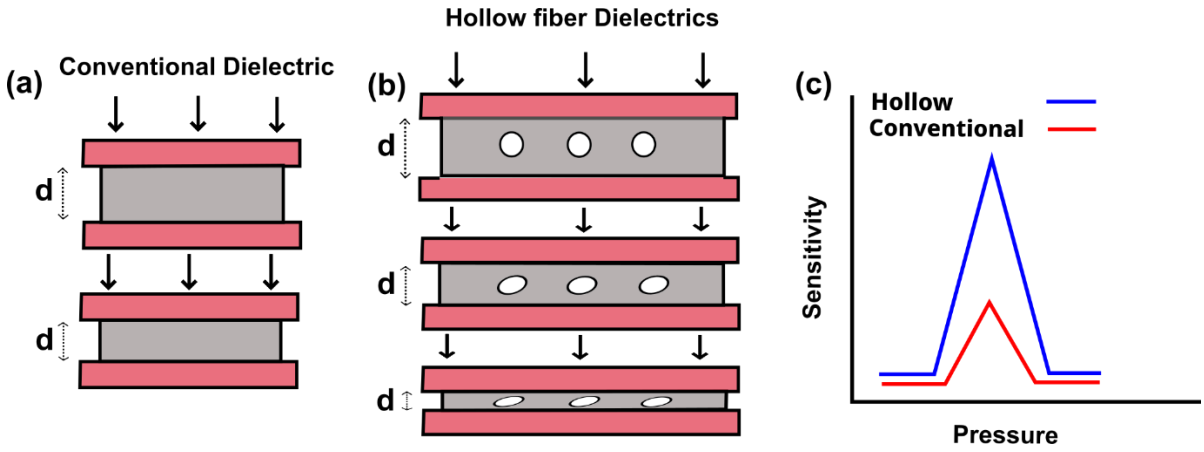

Figure 1 (a) shows a conventional planar dielectric with low compressibility (b) shows a hollow fiber dielectric with porous fibers having higher compressibility when pressure is applied (c) shows sensitivity peaks for hollow (blue peak) and planar dielectric (red peak) when subjected to applied pressure.

1.1 Global Research Trends

Global research trends in capacitive pressure sensing have focused on engineering the dielectric layer's structure and composition to boost sensitivity, especially in the low-pressure regime that is relevant for subtle tactile sensing (e.g., human touch, pulses, or gentle object handling). Two broad strategies have dominated: (1) Geometric micro/nano structuring of the dielectric to increase its compressibility, (2) Material enhancements to increase the dielectric permittivity or dielectric response to pressure. The first strategy includes the use of micro-patterns i.e., pyramids, grooves, pillars, foam or sponge-like porous dielectrics, and fibrous networks that incorporate air voids [7][8]. The second strategy involves high-permittivity composites, e.g., incorporating ceramic or conductive nanoparticles into a polymer that create electric double layers under pressure [9], [10]. Many of the highest sensitivities reported have come from combining these approaches. For instance, using a porous elastomer infused with high-dielectric particles or a hierarchical structure with multiple length-scale porosity [11]. One of the studies fabricated a hierarchical microporous dielectric scaffold via melt electro-writing. It has achieved an exceptionally high sensitivity of 3.13 kPa^{-1} at very low-pressures (less than 1 kPa) by providing multi-level deformable pores [12]. With regard to material, another study demonstrates that incorporating ceramic fillers like barium titanate (BT) and calcium copper titanate (CCTO) into a polydimethylsiloxane (PDMS) matrix significantly enhances the composite's dielectric permittivity [13]. Such hierarchical designs offer a graded mechanical modulus (soft response at small strains, stiffer at large strains) to maintain sensitivity over a broad range. However, those operate on a different mechanism and can have trade-offs in complexity and response time. The mainstream trend for simplicity and fast response has been

to exploit geometrical nanostructures in conventional dielectrics. Hence, this project explores the electrospinning technique to develop nanofibers as dielectric surfaces for flexible capacitive sensors. Electrospun nanofibers have high surface to volume ratio and inter-fiber air pockets which compress under pressure and show high sensitivity [9]. However, coaxial fibers can take this a step further by incorporating air gaps inside the fibers, thereby making them more deformable and boosting sensitivity.

The global market for flexible pressure sensors is experiencing significant growth driven by increasing demand in wearable electronics, healthcare monitoring systems, and smart devices. The capacitive sensor market is projected to experience steady growth from 2022 to 2032, with the total market size increasing from USD 28.8 billion in 2022 to over USD 40 billion by 2032 as shown in Figure 2. This upward trend reflects the rising demand for sensing technologies across a range of industries including consumer electronics, automotive, healthcare, and industrial automation. Among the various sensor types, touch sensors and motion sensors consistently lead in market share, driven by their widespread use in smartphones, wearable devices, and smart interfaces. Proximity and position sensors are also gaining traction due to their crucial role in automotive safety systems and robotics. The growth of humidity, temperature, and pressure sensors indicates increasing emphasis on environmental monitoring and smart manufacturing. The proliferation of connected devices and the shift towards automation and intelligent systems have made capacitive sensors essential for accurate, reliable, and energy-efficient sensing. Their ability to detect even minute changes in capacitance without physical contact enhances durability and responsiveness, making them vital components in the future of smart technology ecosystems [14].

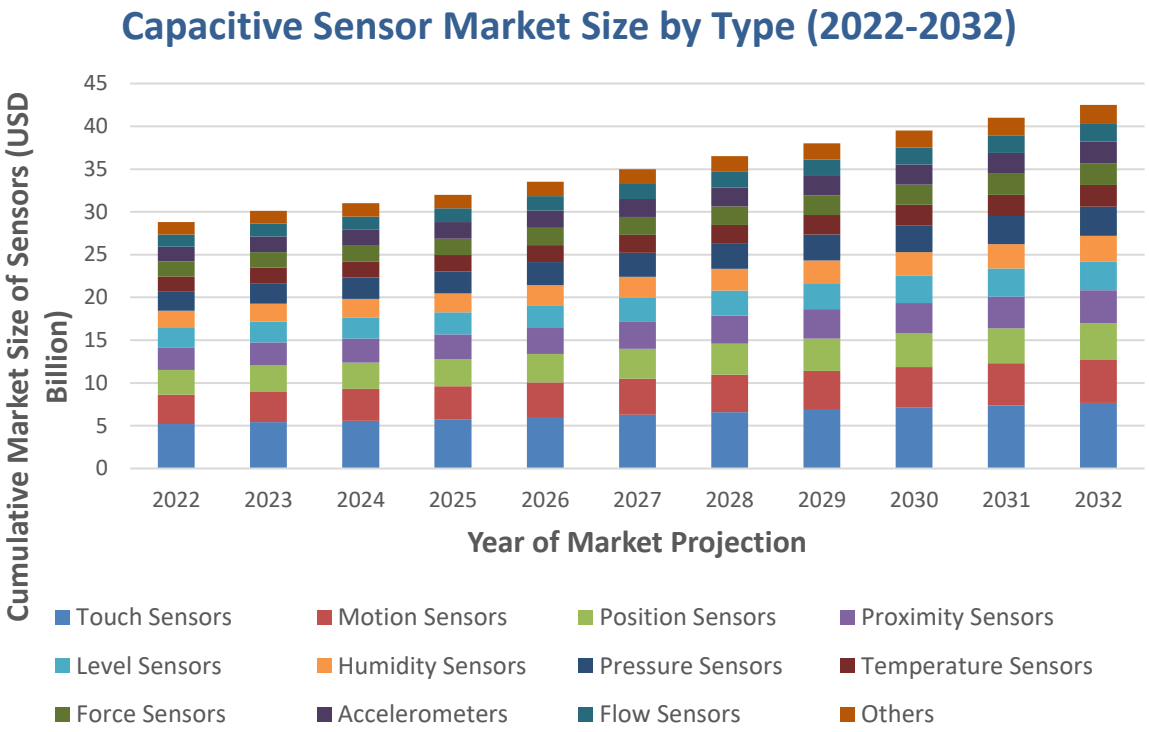

Figure 2 Estimated values derived from a market chart published by Global Market Insights projecting the increase in the market size of capacitive pressure sensor from 2022 (28.8 billion $) to 2032 (over 40 billion $). The estimation was made for academic representation purposes using visual scaling methods [14].

1.2 Electrospinning Technique

Electrospinning is a nano fabrication technique to develop fibrous surfaces having porosity and large surface area. It employs high voltage on the polymer melt which ejects ultrathin stream of spinning fibers. These fibers solidify and are collected on the oppositely charged collector plate as non-woven, randomly oriented and interconnected fiber networks. The scope of this work discusses mainly two approaches of electrospinning Single fiber and Coaxial electrospinning. Single fiber utilizes single polymer fiber with solid core. It exhibits high sensitivity due to high surface area and air trapped in inter-fiber voids [10]. However, their performance is limited due to the lack of inner fiber compressibility. Coaxial electrospinning utilizes two polymer solutions, i.e., sheath and core solution. These two polymers are spun simultaneously from a concentric nozzle. The core material is being removed later, leaving behind the hollow core. This inclusion of hollow core amplifies charge storage capacity, resulting in improved performance for precise pressure measurements [15]. In this work, a comparative analysis of coaxial and control sensors is performed in terms of their sensitivity at low-pressure regimes. Coaxial electrospun fibers are synthesized by electrospinning and used

as a dielectric surface for capacitive sensors. Similarly, the control nanofibers are synthesized and used as a reference in performance measurement. Characterisation of hollow fibers confirms the hollow core and hence showing core-sheath structure. Several tests are performed, which measure sensitivity, responsiveness and practical demonstration.

1.3 Sensitivity of a Capacitive Sensor

Sensitivity in capacitive sensors quantifies how responsively the capacitance changes with applied pressure. In general terms, sensor sensitivity is defined as the change in output per unit change in input stimulus. For a pressure sensor, this may be expressed as the capacitance change per unit pressure, and two definitions are commonly used in the literature. One is the normalized sensitivity defined as the relative change from the baseline capacitance [16][17].

$$S = \frac{\frac{\Delta C}{C_0}}{\Delta P} \quad (1)$$

where ΔC is the change in capacitance, C_o is the baseline capacitance, and ΔP is the applied pressure. It has units of kPa^{-1}. The other is the absolute sensitivity which directly measures the raw capacitance variation per pressure. It has the unit of pF kPa^{-1} or FPa^{-1} [18].

$$S = \frac{\Delta C}{\Delta P} \quad (2)$$

Each definition has its context, i.e., normalized sensitivity measures comparisons between devices with different baseline capacitances, while absolute sensitivity conveys the magnitude of the output signal change. For instance, a recent flexible capacitive sensor based on electrospun nanofibers reported a normalized sensitivity around 0.28 kPa^{-1} in the low-pressure range [19]. In contrast, some textile-based capacitive sensors or large-area devices might emphasize absolute changes (e.g., a few pF per kPa) when the baseline capacitance is very low. In this thesis, sensitivity will primarily be discussed in the normalized sense as this is the prevalent metric in capacitive sensor research. It is important to note that the sensitivity of a capacitive sensor is not a single fixed value across all pressures. However, it varies with the pressure. Often, sensitivity is highest in a certain low-pressure range and then declines once the structure's compressible features are exhausted. Consistent definition and reporting of sensitivity are crucial for comparing sensor performance across studies. This project addressed several critical challenges in the development of flexible capacitive pressure sensors, particularly those related to enhancing sensitivity at low-pressure, maintaining performance

across a broad pressure range, and achieving structural reproducibility. By employing coaxial electrospinning to fabricate hollow nanofibers with tuneable core–shell structures, this study systematically investigates how internal fiber porosity influences the dielectric response, mechanical recoverability, and long-term stability of the sensor. The experimental work presented further explores the comparative performance of hollow versus solid nanofiber mats, hence offering insights into how geometric tuning at the fiber level can overcome conventional trade-offs between sensitivity and mechanical robustness.

Disclosure:

Artificial Intelligence was used in some parts of this thesis to assist with language refinement, rephrasing technical content for clarity, and organizing structure in some sections. All scientific analysis, experimental interpretation, and original research design were independently conducted by the author. The content has been critically reviewed and verified to ensure academic integrity. The use of AI in this work complies with the University of Turku's policy on AI in teaching and studying (UTU AI Policy 3/2023)

Parts of this thesis have been previously published in the IEEE Journal on Flexible Electronics, where the author is listed as a co–first author:

> S. Siddique, A. Barua, R. Gogoi and V. Sharma, "Electrospun Hollow Nanofiber Surfaces as Dielectric Mediums for Highly Sensitive Flexible Capacitive Pressure Sensors in Low Pressure Regimes.", *IEEE Journal on Flexible Electronics* (2025), DOI: 10.1109/JFLEX.2025.3577111.

2 Literature Review

2.1 Electrospinning Technique for Nano Fabrication

Electrospinning uses a high voltage electric field to draw a polymer solution into a thin fiber mat. A typical setup has four parts: a high voltage power supply, a syringe pump, a spinneret (syringe with a metal needle), and a collector. The polymer solution is fed at a controlled flow rate into the needle. At a certain voltage the liquid start accumulating at the tip of the needle and start forming a Taylor cone. When electrostatic repulsion overcomes surface tension, thin charged jet is ejected. The jet thins and whips as solvent evaporates, depositing solid nanofibers on the collector [20]. There are certain key process parameters which strongly influence fiber morphology. Understanding the effect of various parameters on both single-shell and coaxial electrospinning is inevitable for optimizing fiber morphology, mechanical integrity, and functional performance.

2.1.1 Effect of Polymer Concentration and Viscosity

Polymer concentration directly impacts solution viscosity and determines whether a polymer solution is spinnable. In single nozzle electrospinning, too low a concentration leads to electro spraying, while too high causes excessive viscosity that prevents jet formation. Similarly, in coaxial electrospinning, the concentration of both core and sheath solutions must be optimized. A low-viscosity sheath leads to Rayleigh instabilities and bead formation. Increasing sheath viscosity suppresses such instabilities, resulting in smoother fibers [21]. Notably, higher sheath polymer concentration tends to increase fiber diameter. Increasing the core concentration also results in greater core and overall fiber diameters, often leading to morphological transitions, such as from circular to ribbon-shaped cross-sections [22]. Such effects depend heavily on the miscibility and volatility of solvents used.

In coaxial electrospinning, core concentration also significantly affects the resulting fiber morphology. For example, an increase in core concentration results in increased core diameter and overall fiber size. In some cases, the fiber cross-sections shift from circular to ribbon-like, particularly when the volatility and miscibility between core and sheath solutions are imbalanced. Additionally, high core flow rates paired with appropriate sheath viscosity may stabilize the core and prevent droplet formation. Overall, balancing the viscosities of both solutions is essential for achieving structural integrity and functional fibers.

2.1.2 Effect of Miscibility and Interfacial Interaction

For coaxial electrospinning, it is desirable to have low interfacial tension between the core and sheath [23]. When the two solutions are miscible, the interfacial tension becomes negligible. This phenomenon is demonstrated by electrospinning polyethylene oxide (PEO) in water–ethanol mixtures, using dyes to visualize the interface. Despite miscibility, a sharp boundary was observed due to the slower diffusion of polymers compared to the rapid electrospinning process [24]. However, other investigations noted possible diffusion and even complete mixing between core and sheath solutions [22].

In contrast, immiscible core–sheath systems are often employed when hollow fibers are desired, as the sheath solidifies before any significant mixing can occur. This allows selective removal of the core post-spinning, enabling fabrication of hollow structures. Li and Xia, for example, achieved hollow silica fibers using immiscible solvents, where solvent evaporation led to phase separation, supporting pore and cavity formation inside the fibers. Therefore, the interplay between miscibility, volatility, and solvent compatibility governs both morphological outcomes and application-specific fiber design [25].

2.1.3 Effect of Applied Voltage

In electrospinning, the effect of applied voltage on fiber diameter is complex and depends upon which phenomenon is dominant. In single nozzle systems, increasing the voltage beyond a critical threshold enhances Coulombic repulsion, stretching the jet and reducing fiber diameter [26]. However, the intensified electric field can also draw more solution toward the collector, potentially increasing the diameter. The resulting trend may thus be nonmonotonic, depending on which effect prevails [27].

In coaxial electrospinning, only a narrow voltage range yields stable core–sheath structures. At low voltages, jet formation is not enough, while excessively high voltages can destabilize the coaxial structure by entraining more solution than the flow rate supplies, hence causing core–sheath separation and multiple jets [28]. The optimal voltage range is highly dependent on solution properties and system configuration. Within the stable jetting range, increasing voltage

generally reduces both the core and overall fiber diameters due to enhanced charge density and electrostatic stretching, while sheath thickness remains relatively unchanged [29], [30].

2.1.4 Effect of Flow Rate

In coaxial electrospinning, precise control of the core and sheath flow rates is essential for producing stable and well-defined core–sheath fibers. Increasing the sheath flow rate generally leads to a larger overall fiber diameter. However, after a certain threshold, the core may segment [31]. Conversely, a sheath flow rate that is too low can result in incomplete encapsulation or core breakup into droplets.

Increasing the core flow rate tends to enlarge both the core and overall fiber diameters, primarily due to the greater supply of core material and die-swell effects associated with viscoelastic fluids [32]. However, when the core solution lacks viscoelasticity, changes in core flow rate have minimal impact on fiber diameter due to the reduced die-swell phenomenon [33].

2.1.5 Effect of Electrical Conductivity

The electrical conductivity of the core and sheath solutions significantly influences charge distribution and jet formation during coaxial electrospinning. In a compound droplet, induced charge distributes based on the relative conductivity of each component. When the sheath solution is more conductive, surface charges tend to accumulate at the sheath-air interface, effectively making the sheath the primary driving phase. In this scenario, Coulombic forces act predominantly on the sheath, which in turn entrains the core into the jet [34].

Conversely, when the core is more conductive, it becomes the active component that drives the jet, pulling the sheath along with it. For example, one of the studies demonstrated coaxial electro spraying of olive oil as the sheath was only possible when a conductive aqueous solution was used as the core [35]. This setup enabled successful jet formation, highlighting the crucial role of core conductivity. However, it was also observed that when the core's conductivity exceeded that of the sheath, the electric field could accelerate the core more rapidly than the sheath, occasionally disrupting the formation of a uniform core–sheath structure [31].

2.1.6 Tip-to-Collector Distance (TCD)

Tip-to-collector distance (TCD) critically impacts fiber morphology by regulating the time available for solvent evaporation. In coaxial electrospinning, sufficient TCD ensures both core

and sheath solvents evaporate effectively, minimizing bead formation and fusion. If the TCD is too short, incomplete solvent evaporation can lead to fiber merging or wet deposition.

On the other hand, excessively long distances may weaken the electric field, destabilize the jet, and result in non-uniform or broken fibers. The optimal TCD must, therefore, strike a balance between providing sufficient flight time and maintaining electrostatic force strength. Particularly for coaxial systems involving multiple solvents or viscous cores, a carefully selected TCD enhances fiber uniformity, integrity, and functional performance [36].

Table 1 shows the effect of different parameters on Control and Coaxial Electrospinning fibers [25][28][32].

Parameters	**Description**	**Effect in Single Nozzle Electrospinning**	**Effect in Coaxial Electrospinning**	**Additional Notes**
Polymer Concentration & Viscosity	Controls chain entanglement and fluid stretching through polymer concentration and solution viscosity.	Higher concentration yields thicker, smoother fibers; too low causes beads or electro spraying.	Higher sheath/core concentration increases fiber and sheath/core diameter; imbalance can disrupt core-sheath structure. Lower viscosity causes Rayleigh instabilities and bead formation.	Ensure concentration above entanglement threshold. maintain viscosity balance in core-sheath systems.
Miscibility & Interfacial Interaction	Degree of solvent compatibility between core and sheath, affecting interfacial tension and mixing.	Not applicable	Partial miscibility stabilizes core-sheath; full miscibility can dissolve interface; Complete immiscibility is preferred in Coaxial hollow fibers	Partial miscibility is often ideal for hollow or distinct core-shell fiber formation.
Applied Voltage	Electric field strength driving jet formation and stretching.	Increased voltage decreases fiber diameter up to a point; too high causes jet instability or bead formation.	Narrow voltage range yields stable core-sheath structure; Higher voltage generally reduces fiber diameter; too high destabilizes coaxial jet and causes core-sheath separation	Maintain within optimal voltage range to ensure stable jet and morphology.
Flow Rate	Volume of solution fed per unit time through nozzle.	Higher flow increases fiber diameter and bead risk; very low flow may cause jet instability.	Higher sheath flow increases overall diameter; higher core flow increases both the core and	Core-to-sheath ratio is critical to maintain encapsulation and uniformity.

			the sheath diameter	
Electrical Conductivity	Solution ability to carry charge, affecting jet acceleration and stability.	Higher conductivity reduces fiber diameter and improves uniformity; low conductivity causes bead defects.	Higher conductivity in sheath stabilizes jet; high core conductivity can stretch core and can also destabilize jet.	Controlled conductivity enhances fiber thinning and stability in both techniques.
Tip-to-Collector Distance (TCD)	Distance travelled by jet before reaching the collector, affecting drying and morphology.	Longer TCD gives thinner, more solid fibers; too short causes wet, fused, or beaded fibers.	Longer TCD helps solvent evaporation in both layers; too short may not be enough for evaporation and causes sheath fusion.	Crucial to balance solvent removal and electric field strength for fiber integrity.

2.2 The Importance of Dielectric medium in Capacitors

The performance of a capacitor is intrinsically governed by its dielectric layer which is sandwiched between two electrodes. The capacitance is stated by the equation [37]:

$$C = \frac{\varepsilon_o \varepsilon_r A}{d} \qquad (3)$$

where ε_0 is the vacuum permittivity and ε_r is the relative permittivity of the dielectric material, A is the overlapping area of the electrodes and d is the distance between the electrodes. The dielectric material is arguably the most crucial component in capacitive pressure sensor performance. Its intrinsic properties such as dielectric constant, nano structure, porosity, thickness, compressibility influence the change in capacitance under pressure stimuli. A highly compressible dielectric layer offers more deformability under slight pressure, hence showing higher change in capacitance and thus higher sensitivity.

Commonly used dielectric materials in flexible sensors are PDMS, polyurethane (PU), Polycaprolactone (PCL) and Ecoflex. PDMS has moderate permittivity ($\varepsilon_r \approx 2.5–2.8$) which limits the desired mechanical response for detecting very low-pressures. To overcome these challenges, several researches are taking place which are introducing micro and nano structures in the dielectric material [7]. Micropatterns such as pyramids, domes, pillars or wrinkles make the dielectric layer more compliant under small pressure [38]. Wan *et al.* demonstrated a lotus-leaf mould to produce PDMS micro towers and achieved approximately 1.2 kPa^{-1} sensitivity

below 1 kPa [39]. The presence of air voids inside the microstructures induces compressibility. It also shows linear response over a range of pressure. However, one drawback is that patterned surfaces require complex fabrication procedures which eventually collapse under high-pressure or over a series of pressure. Similar kind of approach towards introducing air voids is sacrificial templating. It involves fabrication of the porous PDMS dielectric layer with a hole array, a two-step process, beginning with the synthesis of the porous PDMS material (see Figure 3a) followed by precise laser ablation. As illustrated in Figure 3b, a carbon dioxide laser was used to ablate the porous PDMS surface, forming a patterned array of circular holes designed as a 6 × 6 matrix. The inter-hole spacing (d) served as a critical design parameter for optimization. Laser ablation was carried out using a power of 30 W and a scanning speed of 200 mm/s, with the hole depth modulated by controlling the number of ablation passes. Two ablations under these settings achieved a depth of approximately 2 mm, matching the film thickness. This method yielded a uniform and structurally stable dielectric layer, suitable for integration into flexible capacitive pressure sensors. It results in achieving high sensitivity around 1.15 kPa^{-1} under low-pressure ranging 0-1 kPa [40]. However, the trade-off can be mechanical stability or hysteresis. The porous membranes can show non-linear response under same pressure provided the holes collapse. Also, attention needs to be done while removing the pin while creating holes as it can tear the membrane. In general, porosity is an effective way to boost compressibility and thus showing high sensitivity at low-pressure regimes.

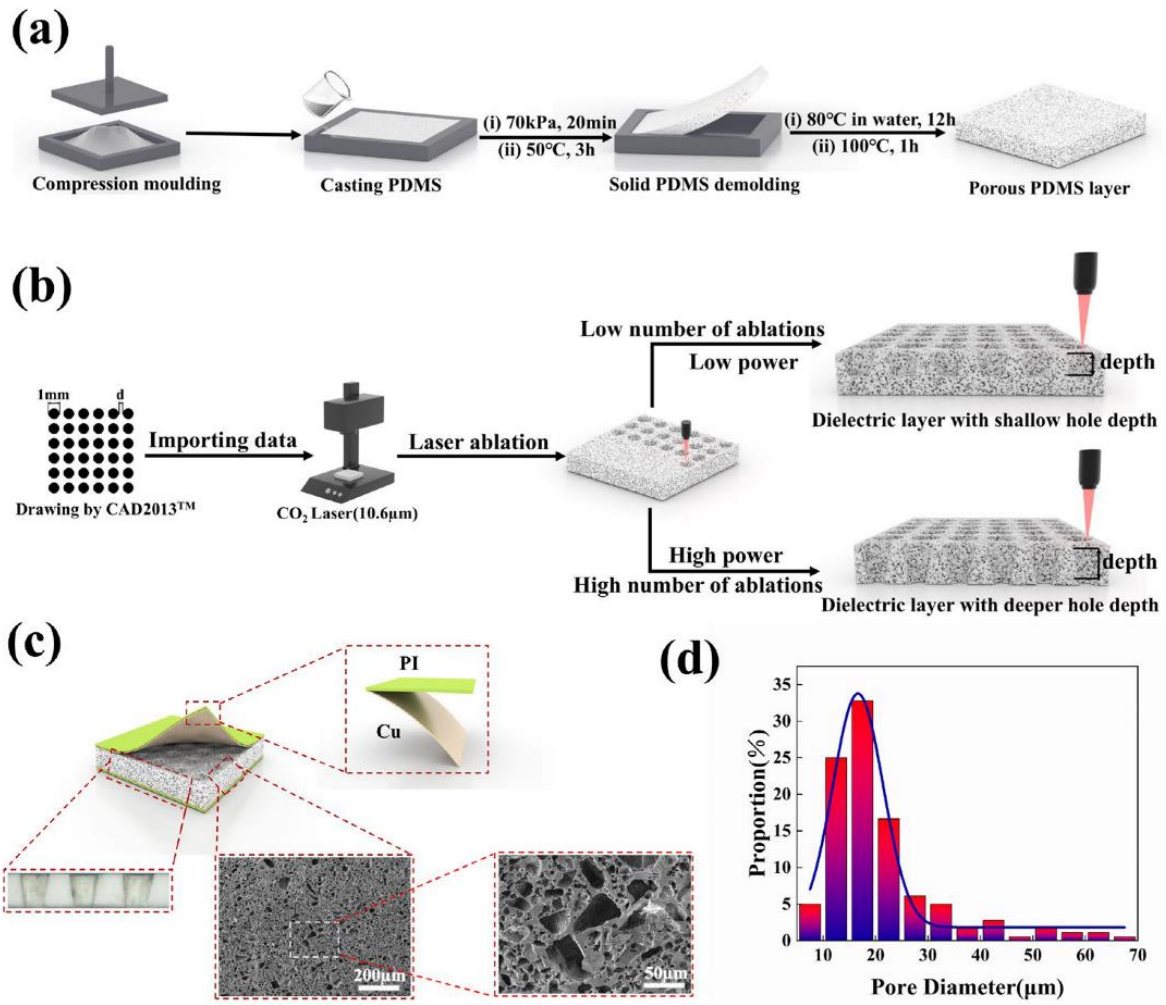

Figure 3 (a) shows the preparation process of a porous PDMS dielectric layer. (b) Detailed schematic of the laser ablation method. (c) Visual overview of the flexible capacitive pressure sensor, featuring an optical microscope image of the hole array and SEM imaging showcasing the microporous structures. (d) graph shows the size distribution of micropores within dielectric layer [40].

Another technique is to enhance the base permittivity by adding high dielectric constant fillers such as ceramic nanoparticles. For instance, a $BaTiO_3$–PDMS composite having a gradient micro-cone structure achieved a sensitivity of approximately 1.69 kPa^{-1} in the 0–50 kPa range, without compromising its mechanical compliance [9]. Similarly, Guo *et al.* fabricated a sensor by printing ~3.75 wt% carbon nanotubes (CNTs) into a PDMS matrix exhibited even higher sensitivity i.e., 2.9 kPa^{-1} at very low-pressures ranging 0–450 Pa. The CNTs/PDMS composite dielectric layer was prepared by dispersing CNTs into a PDMS matrix, followed by three-roll milling for uniform mixing. The mixture was spin-coated onto a silicon mould with pyramidal microstructures and cured at 70 °C for 2 hours. The cured layer was peeled off and integrated into a flexible capacitive pressure sensor by assembling it between screen-printed electrodes on Polyethylene Terephthalate (PET) substrates as shown in Figure 4. This process enabled the development of highly sensitive pressure sensors [41]. Additionally, silver nanowire AgNWs–

PDMS composites have been reported with sensitivities near 0.83 kPa^{-1} under a pressure of few pascals. These studies highlight how material choice and structural design can be tailored to achieve high sensitivity across different pressure regimes. However, introducing fillers in the elastomers reduces its stretchability and hence there is a trade-off between achieving high relative permittivity and flexibility.

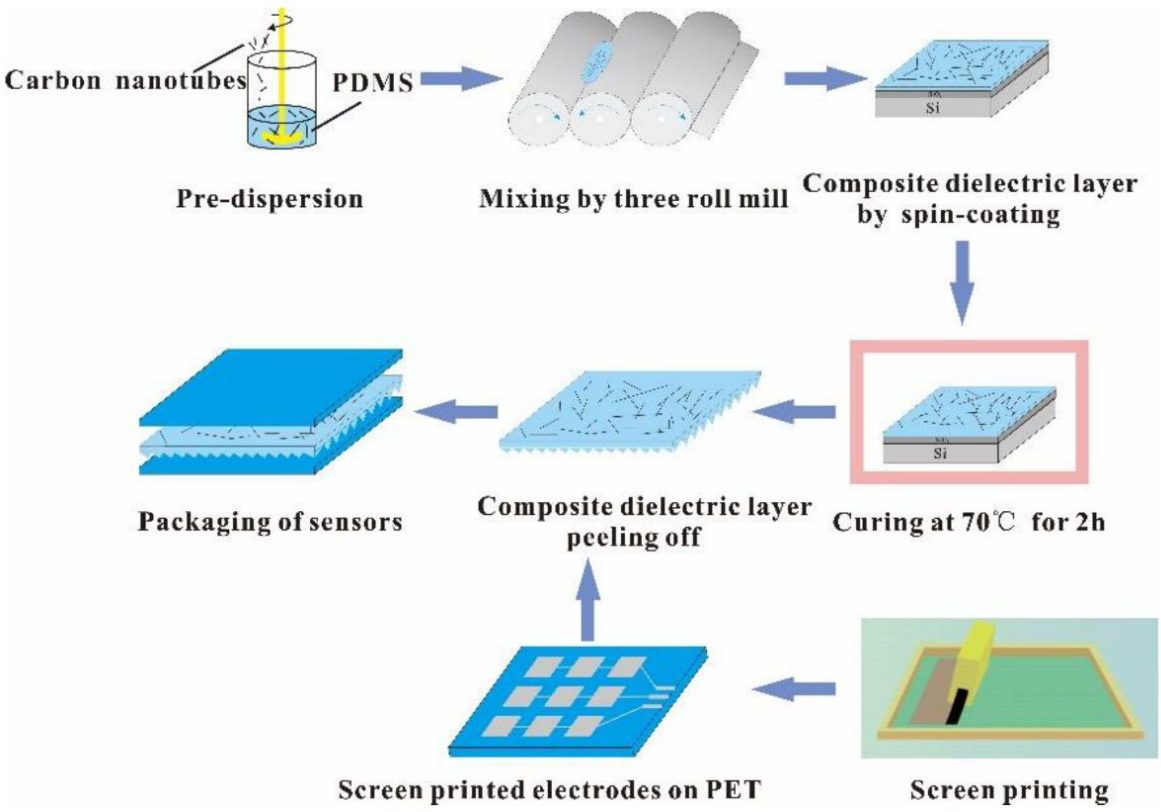

Figure 4 shows schematic of the fabrication of the capacitive pressure sensor by using CNTs [41].

Zhu *et al.* used fibers as a flexible sensor dielectric, using an electrospun Polyimide (PI) nanofiber mat as the dielectric layer. Due to fibrous structure, the sensor showed a superior sensitivity of approximately 2.2 kPa^{-1} in the extremely low-pressure range 3–4 Pa. The high sensitivity in this design is subjected to its relatively high intrinsic dielectric constant combined with the nanofiber membrane porosity and compressibility [42]. However, the sensitivity tapered at high-pressure range because porosity compacted at high-pressures. Nonetheless, such flexible sensors are utilized in detecting subtle physiological monitoring. An interesting case in which porous membrane and fillers are used to enhanced sensitivity is worth mentioning here. A capacitive sensor is fabricated based on a Thermoplastic Polyurethane Urethane rubber (TPU) electrospun membrane infused with AgNWs as a composite dielectric. The TPU fibers provide elasticity and a breathable scaffold while the dispersed silver nanowires raise the effective dielectric constant and create micro capacitive junctions within the dielectric. The

result was a sensor with remarkably high sensitivity i.e.,7.24 kPa^{-1} below 1 kPa. and a very low detection limit of approximately 9 Pa. The AgNWs not only increased baseline capacitance but also made the dielectric permittivity "easily alterable" under pressure due to changes in nanowire orientation and spacing. Importantly, this sensor maintained its performance over 1000 cycles and was highly breathable, making it suitable for wearable applications This example illustrates how adding conductive or high dielectric constant fillers to electrospun fibers can amplify sensitivity, though care must be taken to keep filler content low enough to avoid electrical percolation [43].

2.3 Charge Formation Mechanism

This project primarily focuses on hollow fiber-based capacitive pressure sensor. Before delving into the charge formation mechanism, it is essential to discuss the theoretical basis for charge storage. The total capacitance, C_{total} in this configuration is given as follows [44];

$$C_{total} = \frac{A}{\frac{d_{in}}{\varepsilon_{in}} + \frac{d_{shell}}{\varepsilon_{shell}} + \frac{d_{out}}{\varepsilon_{out}}} \quad (4)$$

Here, A is the active area of the dielectric medium sandwiched between two electrodes, d_{in} is the inner core thickness (typically air), d_{shell} is the thickness of the polymer nanofiber wall and d_{out} is the outer dielectric spacing between the electrode and the fiber surface. The model also accounts for dielectric porosity.

Charge formation mechanism is schematically illustrated under different pressure conditions (see Figure 5). At zero pressure, the electrode separation is defined by the initial dielectric geometry (including internal air gaps). When the voltage is applied, free charges accumulate on the electrodes, inducing an electric field across the dielectric medium. As pressure increases the dielectric layer compresses – effectively reducing d and any air voids within it collapse, hence increasing the relative permittivity ε_r. Both smaller d and higher relative dielectric ε_r lead to a larger capacitance C, i.e., a positive capacitance change. At high-pressure, the deformable features of the dielectric (such as air gaps or porous structures) may be largely eliminated (squeezed out), so the capacitance approaches that of a solid, fully compressed dielectric. In this saturation regime, further pressure causes little additional deformation, and thus the rate of capacitance change diminishes. This behaviour highlights a key design challenge i.e., to enhance sensitivity at low-pressures while avoiding early saturation at higher pressures.

Charge formation is intended as a qualitative way to describe the additional polarization and bound charges that arise from the hollow fiber geometry. Specifically, the coaxial hollow fibers create a very large internal surface area due to polymer–air interfaces compared to control fibers. Under an applied voltage (as in a capacitive sensor) or mechanical pressure, dielectric polarization occurs at these interfaces: bound charges accumulate on the internal surfaces of the hollow fibers. We referred to this as increase in "charge formation". In other words, the hollow structure allows additional polarization charge to build up inside the dielectric, which contributes to improve dielectric properties. Moreover, the hollow fibers are much more deformable than solid ones. Under applied pressure, the thin fiber walls bend and internal air gaps collapse easily, leading to greater geometric deformation and, consequently, a larger change in capacitance that results in higher sensitivity. The dominant factor in our sensor is geometrical alteration due to the mechanical deformation of PCL sheath [45].

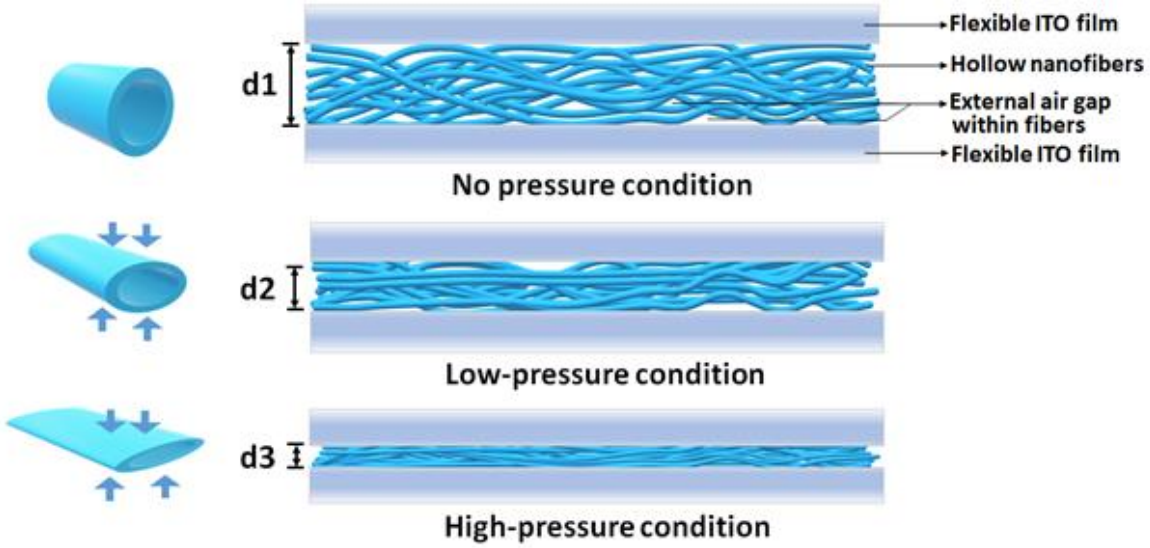

Figure 5 Mechanism of the capacitive pressure sensor at no pressure, low-pressure and high-pressure condition.

2.4 Performance Metrics

In addition to high sensitivity, an effective pressure sensor must exhibit fast response, low hysteresis, and good stability over repeated use. The term, Hysteresis, can be explained as difference in sensor output in loading and unloading curves, is generally minimal in capacitive sensors relative to resistive ones, because the sensing mechanism purely relies on geometric and permittivity changes rather than frictional contacts or piezoresistive material rearrangements. Nanofiber-based capacitive sensors due to their low mass and porous structure allow quick mechanical equilibration, excel in response time. When pressure is applied or

released, the air in the pores can expel and refill rapidly. Reported response times are typically on the order of tens of milliseconds. For instance, a composite TPU nanofiber sensor doped with AgNWs had a response faster than 55 ms [46]. Some devices using ionic liquid-infused nanofibers or hydrogels can achieve even faster electrostatic equilibration. Wu *et al.* reported 18-22 ms response time and excellent stability as shown in Figure 6 [47]. A well designed electrospun dielectric will elastically return to its original form after pressure removal, showing very little residual deformation. However, some nanofiber-based capacitive sensors report negligible hysteretic behaviour over their working range [48]. Small hysteresis can still arise if fibers realign or compact permanently after the first few loading cycles, but this is often mitigated by pre-conditioning the sensor with a few presses. The hollow fiber sensor mentioned here showed minor signal drift only in the first few cycles, after which it stabilized, indicating excellent elastic recovery of the fibrous dielectric.

Another important aspect to measure sensor performance is its durability. Electrospun dielectric sensors have been subjected to thousands or even tens of thousands of loading cycles in the literature to examine signal degradation. For example, the all nanofiber iontronic pressure sensor combines stretchability with sensitivity by using electrospun Polyvinylidene fluoride-co-hexafluoropropylene (PVDF-HFP) and Polyvinyl Alcohol (PVA) layers that form a soft, multi-layered structure capable of efficient ion transport. The durability tests showed stable performance over 5000 repeated cycles as in Figure 6, confirming its reliability for long-term use in wearable electronics and interactive devices [47]. Likewise, a study reported insignificant change in sensitivity after over 1000 pressing cycles on AgNW/TPU fiber sensor. This stability is attributed to the ability of fiber to recover shape and the lack of permanent buckling as long as pressures are within the design range. For example, the TPU nanofiber sensor continued to function with unchanged sensitivity even after being bent 1000 times [46]. These findings illustrate that nanofiber-based capacitive sensors can be engineered for excellent robustness. However, it is worth noting that environmental factors like humidity can affect stability if the polymer is hydrophilic e.g., PVDF or PI fibers might absorb moisture, slightly altering dielectric properties. Encapsulation or hydrophobic surface treatments are thus common to ensure long term signal stability and to protect the fibrous layer from environmental degradation. Overall, with proper material choices and encapsulation, electrospun dielectric layers enable durable sensors that maintain their performance over prolonged cyclic loading.

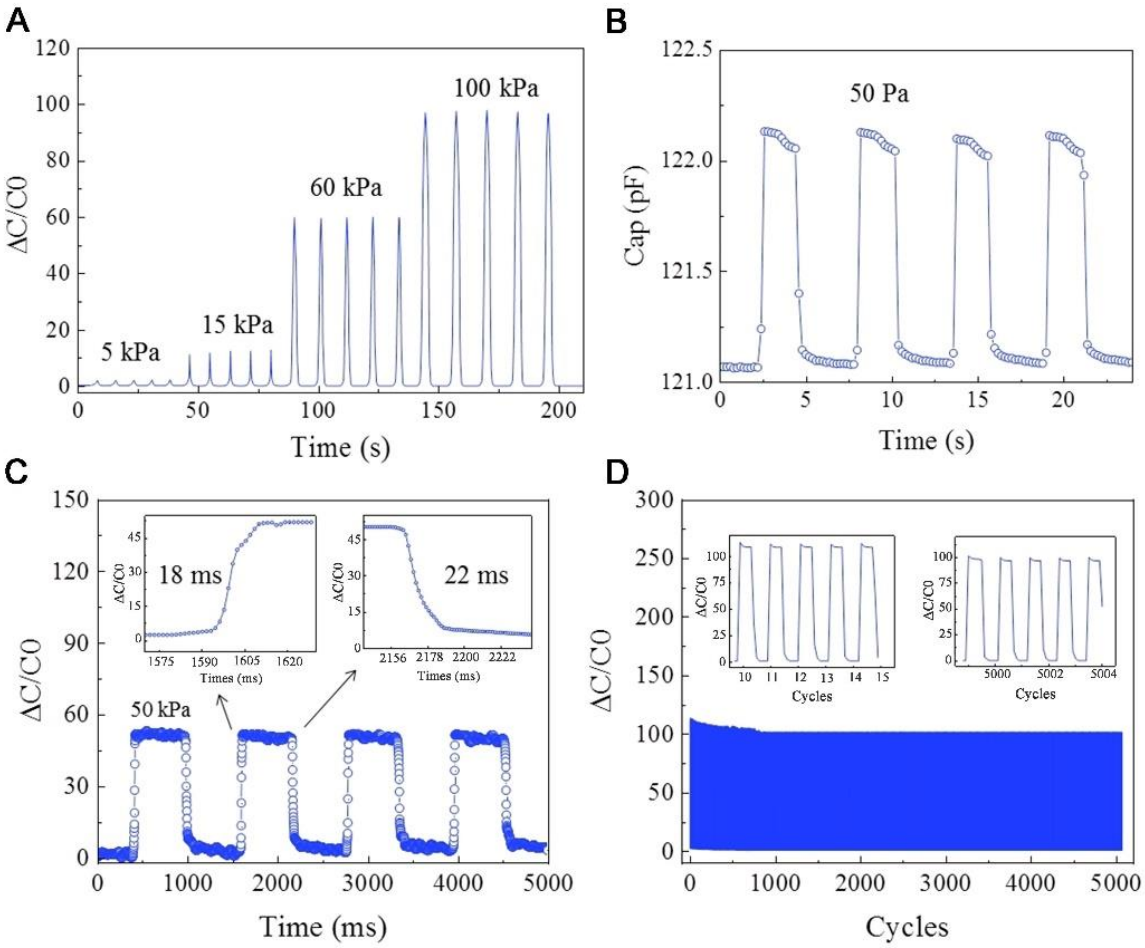

Figure 6 shows the sensing performance of the optimized stretchable all-nanofiber iontronic pressure sensor (SNIPS) (a) the dynamic capacitance response under varying pressure levels. (b) limit of detection (LOD) test. (c) Illustrates the transient response to a 50 kPa (d) durability over 5000 cycles at 250 kPa [47].

2.5 Design Optimization and Trade-offs

While electrospun nanofiber dielectrics offer clear benefits, designers must consider several trade-offs to meet specific application requirements. One primary consideration is fabrication complexity versus performance. Synthesizing core–shell fibers typically requires a coaxial electrospinning setup (dual nozzle spinneret with two solvents) which is more complex than single nozzle electrospinning of solid fibers. In addition, coaxial electrospinning involves multiple parameters to attain the desired fibers. It also requires optimization of viscosity, electrical conductivity, evaporation rate, miscibility, interfacial tension, polymer concentration etc. of sheath and core. This added complexity can be justified by the performance gains. However, if the application does not require extreme sensitivity at very low-pressures, a simpler solid fiber membrane might be preferred for ease of manufacture and reproducibility. Similarly, introducing fillers like AgNWs or nanoparticles into fibers involves additional material

processing and quality control to ensure uniform dispersion. Too high a filler loading can increase dielectric loss or even create percolation paths that introduce leakage currents, undermining the sensor's stability. Thus, there is an optimal filler concentration that boosts permittivity and sensitivity without excessive trade-offs in electrical insulation or mechanical flexibility. Another factor is sensitivity versus pressure range. As discussed earlier, highly porous or hollow fiber dielectrics excel at low-pressure sensitivity but tend to saturate or flatten out at higher pressures.

Designers must balance the fiber mat porosity and thickness such that the sensor covers the intended pressure range. If the goal is to measure up to 100 kPa, a moderate porosity (or a dual-layer structure combining a porous layer with a more solid support layer) may yield a more linear response across that span. On the other hand, for ultra-low-pressure detection (facial muscle movements, pulse, acoustic vibrations), one might maximize porosity and accept that beyond a few kPa the sensitivity will decline. Some researchers address this by stacking multiple dielectric layers or creating hierarchical structures – for instance, a thin porous nanofiber layer for the initial response and a underneath layer of larger microfibers or foam to bear higher loads (see Figure 7). This can produce a multi-stage response: a steep slope at low-pressure and a gentler slope at higher pressure, extending the dynamic range at the cost of a more complex structure [49][12].

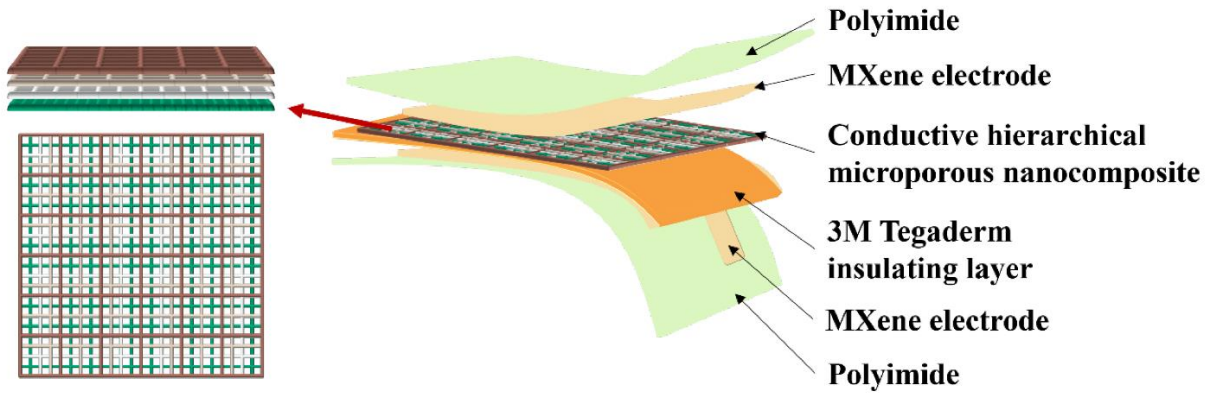

Figure 7 illustrates microporous capacitive pressure sensor having conductive hierarchical microporous nanocomposite layered with insulating layer and sandwiched with MXene electrodes and polyimide substrate [12].

Material selection also introduces trade-offs. A stiffer polymer (like PI or polycarbonate) in fiber form will not compress as easily as a rubbery polymer (like TPU or silicone), which means lower sensitivity but potentially less hysteresis and better operation at high-pressure without collapsing. A very soft fiber (like a thermoplastic elastomer) yields high sensitivity but might experience more viscoelastic creep or require protective encapsulation to prevent

environmental damage. This study PCL (a semi-crystalline, relatively stiff biodegradable polymer) was chosen to ensure the hollow fibers didn't collapse under their own strain, and it provided stable cycling. But if ultimate sensitivity is desired, one might choose a super-soft material or even gel fibers, accepting that the sensor may need more careful handling. Environmental stability is another factor especially with hydrophobic polymers (PVDF, PS) which resist moisture uptake, whereas hydrophilic ones (PVA, gelatin) can swell or degrade with humidity, so the latter might need encapsulation which could reduce the effective sensitivity by constraining the dielectric's expansion [50].

2.6 Materials and Coaxial Fiber Architectures

Recent works have focused on tailoring the core–shell geometry which includes fiber diameter, shell thickness, and pore fraction to maximize sensitivity in the desired range while maintaining structural integrity. For example, a study employed coaxial electrospinning to create hierarchical hollow PVDF (89% porosity) and reported a pressure sensitivity of 1.08V/kPa (piezoelectric mode) [51]. Similarly, coaxial hollow fibers of PVDF loaded with conductive or high K-fillers (e.g., CNTs, $BaTiO_3$) have been reported to further boost the dielectric response by combining microcavity-induced permittivity gains with filler polarization. Qu *et al.* fabricates core–sheath PU fibers with CNTs incorporated into the soft electrode via coaxial wet spinning process. By varying CNT content, the electrode's mechanical modulus is tuned, significantly impacting sensor sensitivity—softer electrodes with optimized CNT ratios enhance the capacitive response as shown in Figure 8. Additionally, controlling the dielectric layer thickness via injection speed allows further sensitivity tuning. The work highlights that simultaneous regulation of electrode modulus (through CNT doping) and dielectric thickness greatly improves sensitivity without complex structural modifications. The resulting sensors show fast response, low hysteresis, and excellent cycling stability, suitable for real-time applications [52]. These diverse material efforts demonstrate that the coaxial electrospinning approach is material dependent: as long as one can co-spin a sheath that solidifies into a fiber and a removable or secondary core, a hollow dielectric structure can be realized. This flexibility has led to composite hollow fibers. This highlights that coaxial hollow architectures can substantially amplify pressure transduction efficiency when nano engineered, outperforming not only flat films but even regular nanofiber dielectrics under small pressures.

A variety of polymer systems and composites have been explored as coaxial nanofiber dielectrics to improve sensor performance beyond what simple PCL fibers offer. Researchers

have investigated electrospun hollow fibers of high-dielectric polymers like PVDF and its copolymers, as well as elastomers such as PU and TPU, often combined with functional fillers. These materials provide higher intrinsic permittivity or greater elasticity for sensor applications. In one notable example, a core–shell TPU/PVDF-HFP nanofiber-based e-skin via coaxial electrospinning was developed. The TPU/PVDF-HFP fibers incorporated ionic liquid in the core, yielding an "ionic dielectric" fiber mat that was highly compressible and also served as a triboelectric generator. As a capacitive sensor, this coaxial mat achieved a high sensitivity of 0.718 kPa^{-1} in the ultra-low-pressure range with a detection threshold down to 7 Pa [53] The PVDF-HFP shell contributed a high dielectric constant and partial piezoelectric response, while the soft TPU core (with ionic content) enhanced deformability and charge induction, exemplifying how multi-material coaxial fibers can be tuned for complementary functional performance.

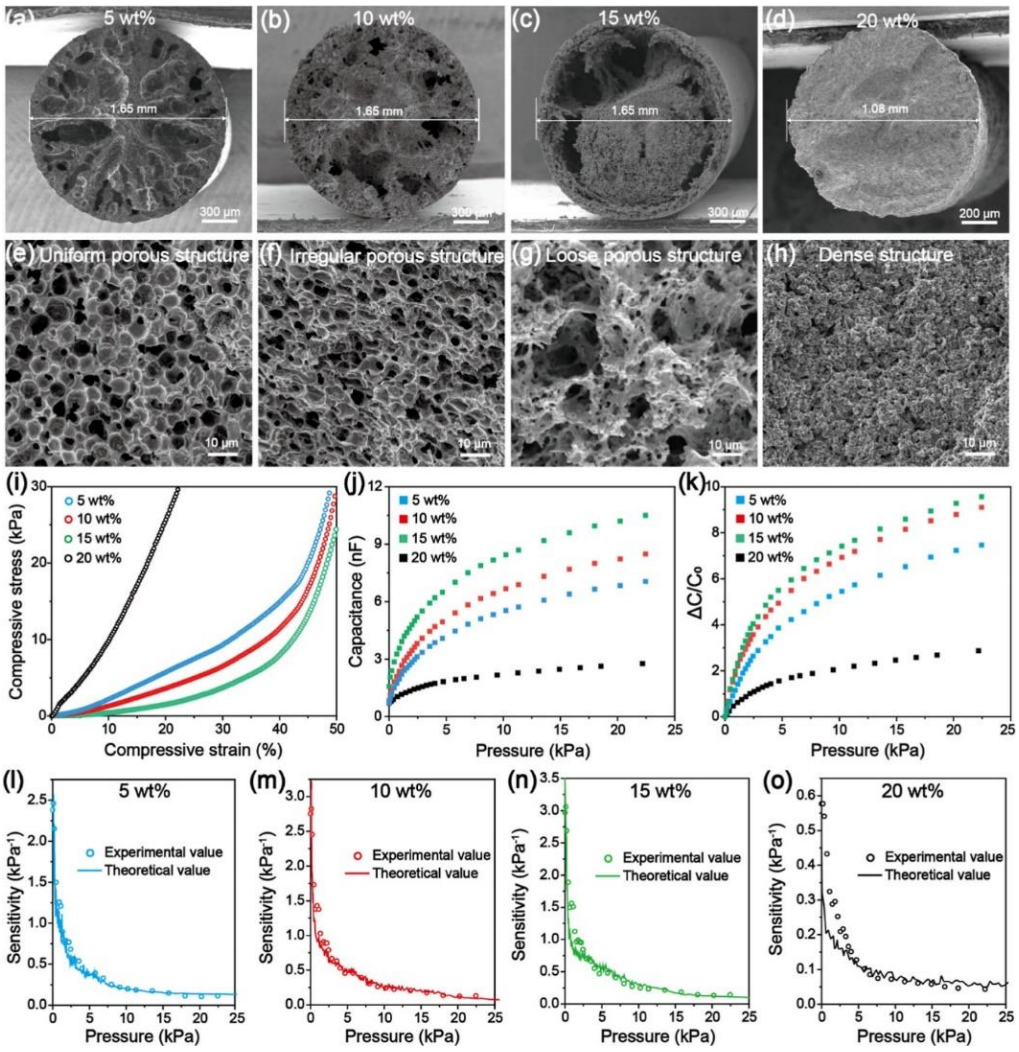

Figure 8 (a-h) shows structural and electrical characterisation of soft electrodes with varying CNT content (5–20 wt%). (l-k) Changes in compressive behaviour and relative capacitive response

demonstrate the impact of CNT ratio on sensor performance and sensitivity (l-o) shows experimental and theoretical mapping of sensitivity with respect to pressure by varying CNT ratio [52].

2.7 Performance Optimization and Structural Resilience

Hollow fiber geometry can be optimized for balancing sensitivity and mechanical resilience. The wall thickness and core diameter directly influence how the fiber deforms under pressure i.e., thinner shells and larger cores have greater capacitance change with pressure but risk structural collapse if too fragile. A recent study combined simulations and experiments demonstrate this trade-off in piezoelectric PVDF fibers. By tuning the coaxial spinneret flow rates, various hollow fractions of PVDF fibers were produced with enlarged inner diameters (i.e., thinner walls) and showed higher deformation under stress, translating to enhanced electrical output (3 times higher piezoelectric voltage than solid fibers). Finite element modelling confirmed that as the hollow core expands, the fiber's effective young modulus drops, allowing it to compress more for a given load and thus generating a larger signal [54].

These findings suggest an analogous benefit for capacitive sensors i.e., a thin-walled hollow dielectric should yield greater capacitance shifts due to its increased compressibility. However, excessively thin shells may buckle or plastically deform under repeated loading. Therefore, an optimal core/shell ratio must be struck to ensure fatigue resistance. In practice, researchers report that well-engineered hollow nanofibers can sustain thousands of loading cycles with minimal performance degradation due to the support of the polymer shell around each air cavity. The robust outer shell in coaxial fibers helps preserve fiber morphology under compression, acting like a spring that rebounds once pressure is released. For instance, the TPU/PVDF-HFP core–shell fibers mentioned earlier retained their sensitivity over prolonged cyclic tests [53]. This resilience is attributed to both the inherent elasticity of the materials and the structural framework of the fibrous network, which distributes strain. Moreover, hollow fiber mats tend to have fast mechanical response times because of their low mass and high porosity that allow quick stress relaxation. Overall, by adjusting fiber diameter, shell thickness, and packing density, researchers can tune the compression mechanics of hollow fiber mats, achieving a balance between high sensitivity and mechanical durability.

2.8 Environmental Stability and Encapsulation Strategies

Environmental factors such as humidity, temperature, and biodegradation can significantly affect nanofiber-based sensor performance, prompting the development of encapsulation and protection techniques. Hollow fiber dielectrics, due to their high surface area and porosity, are

especially susceptible to moisture uptake which can alter their dielectric constant or soften the polymer. To combat this, researchers often encapsulate the fiber layer with thin, flexible coatings that shield it from the environment while minimally impacting its compressibility. A simple yet effective approach is to use thin polymer films or adhesive tapes as packaging. For instance, this study encapsulates PCL nanofiber sensor between layers of transparent cellulose tape, which prevented direct exposure to air and humidity without sacrificing device flexibility. Encapsulation not only stabilizes the sensor in humid conditions but also protects fragile hollow structures from mechanical abrasion or contamination in real-world applications. In harsher environments (e.g., wearable sensors exposed to sweat, or outdoor conditions), more robust encapsulants like silicone elastomers (PDMS) or PU coatings have been used to seal the nanofiber mat. These coatings can be made ultrathin and porous (e.g., microporous PU films) to preserve breathability and touch sensitivity while keeping water out.

Another challenge is the long-term integrity of biodegradable fiber materials like PCL in biologically active surroundings. Studies have shown PCL will gradually hydrolyse or biologically degrade which is undesirable for sustained sensor function [55]. To extend device lifetime, researchers have explored protective barriers and even enzyme inhibitors. Protective encapsulation with an inert film can slow hydrolysis, allowing PCL based sensors to function for extended periods in wet or microbial environments [56]. Overall, combining coaxial nanofiber dielectrics with smart encapsulation strategies is key to preserving sensor performance in the field. The encapsulation must be carefully designed so as not to impede the fiber mat's deformation i.e., using a stretchable overlayer for stretchable sensors, or a vapor-permeable membrane if outgassing of trapped air is needed for fast response. By addressing moisture sensitivity and material longevity in this way, recent works have managed to maintain consistent capacitance readings even in humid, wet, or biologically active conditions, which is crucial for wearable and outdoor sensing applications.

2.9 Comparison of Electrospun dielectrics with other Approaches

Coaxial hollow fiber dielectrics represent one approach among many microstructural designs for capacitive sensors. It is imperative to compare their performance and characteristics with alternatives like porous foams and patterned elastomer surfaces. Micropatterned dielectric layers (such as arrays of micro domes, pyramids, or pillars on silicone rubber) have demonstrated high sensitivities by concentrating strain in small regions. For example, a micro-pyramid PDMS sensor achieved more than 1 kPa sensitivity and fast millisecond response,

along with a broad working range up to hundreds of kPa, by preventing early saturation of contact area. He *et al.* showed the enhanced detection range and long-term stability of the sensor which uses a micro-structured PDMS dielectric layer replicated from the eggshell inner membrane (ESIM), which has a fibrous network structure allowing greater compression and improved sensitivity. The electrodes are made by combining 1D AgNWs tightly wrapped with multilayer 2D MXene sheets, providing rough surfaces and abundant conductive pathways. MXene sheets are produced by etching and delaminating the MAX phase and form uniform, thin films with good dispersion as shown in Figure 9. This structure improves the sensor performance by increasing surface roughness and electrical conductivity [57].

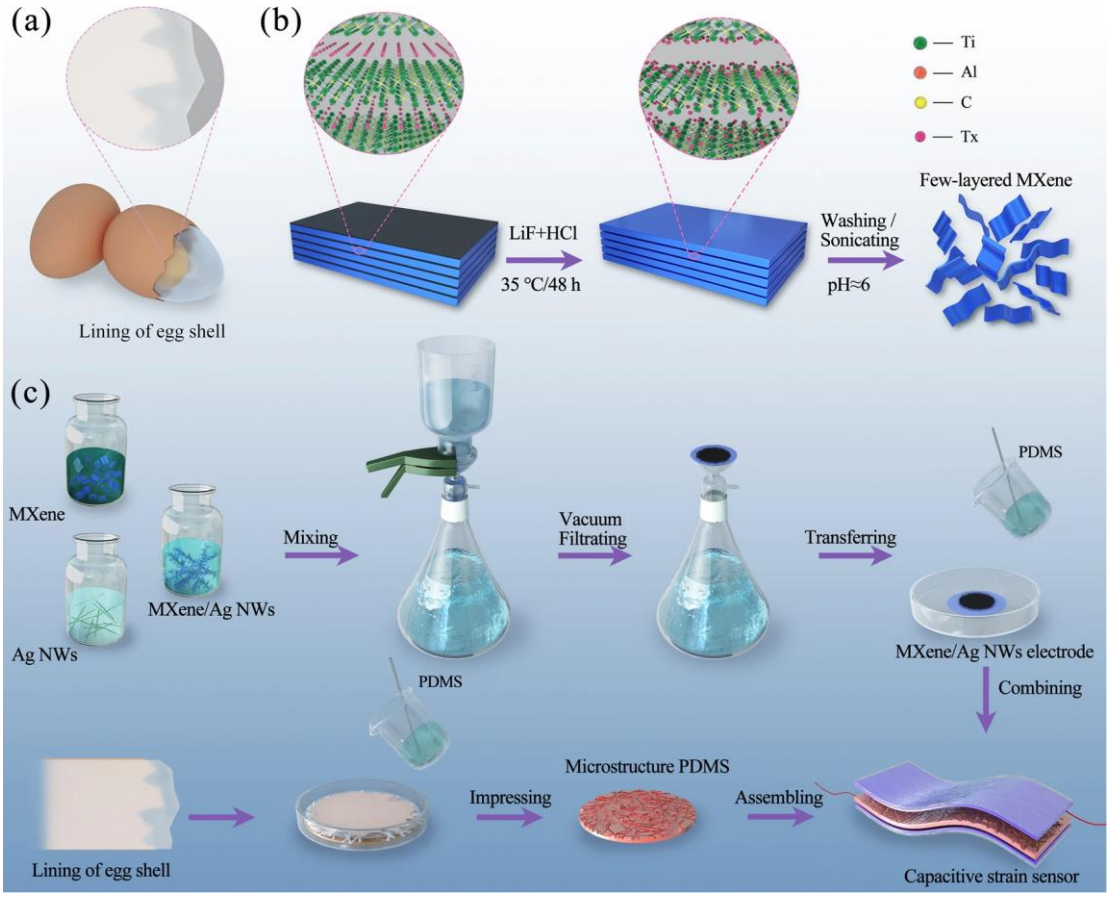

Figure 9 (a) shows structure of the eggshell inner membrane (ESIM) (b) MXene sheet fabrication process (c) Assembly of the flexible capacitive pressure sensor with micro-structured PDMS and MXene/AgNWs electrodes [57].

Hollow nanofiber mats show high sensitivity at low-pressure, but tend to compress fully at lower forces compared to tall micropillars, which limits their linear range. However, fibrous dielectrics offer immediate benefits in simplicity and porosity. Unlike lithographically patterned elastomers, electrospun mats can be fabricated over large areas with ease, and their pores naturally enable air permeability. Compared to bulk foams (e.g., sponge-like PU or PI

foams), hollow fibers provide a more controlled microstructure; the size and distribution of air voids are governed by fiber diameter and packing density which can be tuned via electrospinning parameters. This often leads to more repeatable performance and lower hysteresis than random foams. Indeed, a recent review noted that electrospun nanofiber dielectrics generally show excellent cyclic repeatability over thousands of cycles, whereas some foam-based sensors suffer from gradual compaction [58][53].

Another advantage of hollow fiber mats is their ultrathin form, they can be made as thin as a few tens of microns, whereas achieving a uniformly thin foam or structured elastomer layer can be challenging. This thinness improves conformability when the sensor is applied to curved surfaces (e.g., skin or robotic joints). In terms of sensitivity tuning, coaxial fibers and foams both rely on introducing air gaps to raise compressibility but fibers allow anisotropic architectures (e.g., aligned or layered fiber mats) that foams cannot easily replicate. Foams and patterned elastomers typically sustain larger pressures without damage, since their structures are bulkier. Whereas, hollow fibers might collapse or break if pressed far beyond their design range. Consequently, some of the highest-pressure capacitive sensors (able to detect up to the MPa range) still use structured solid dielectrics rather than hollow fibers [57]. It is also worth exploring some hybrid approaches, for instance, fiber foam composites and fiber reinforced micropatterns to capitalize on the strengths of each microstructure.

In summary, coaxially electrospun hollow nanofibers have carved out a niche in achieving very high sensitivity at low-pressure and excellent flexibility, exceeding other microstructure dielectrics in that regime. Their unique combination of air inclusions, high surface area, and fibrous mechanical support makes them particularly suited for applications like tactile skins, pulse sensors, and subtle pressure changes. Meanwhile, for applications requiring wide pressure ranges or extreme load endurance, designers might combine hollow fibers with more robust microstructures. Comparative studies suggest that no single structure is universally superior – instead, the choice often depends on the target pressure range and environment. Coaxial hollow fibers stand out in the realm of light touch, high sensitivity sensing hence offering a compelling balance between performance and processability. Recent literature confirms that ongoing refinements in their materials and structure continue to push this balance to new heights.

2.10 Literature Gap

Despite significant advancements in the development of flexible capacitive pressure sensors, several critical gaps remain in the literature. Most existing capacitive pressure sensors,

especially those employing solid or planar dielectric layers, suffer from limited sensitivity at low-pressures. This restricts their applicability in detecting subtle tactile stimuli or physiological signals. While some approaches attempt to improve performance through micro structuring or material blending, the dielectric's mechanical compliance and permittivity remain limiting factors. Capacitive sensors with high low-pressure sensitivity often suffer from saturation or mechanical collapse at elevated pressures, leading to poor performance across broader pressure ranges. In this work, a coaxially electrospun hollow nanofiber dielectric is introduced, which enhances mechanical deformability and amplifies capacitive response due to internal air cavities. The resulting sensor exhibits a maximum sensitivity of 1.05 kPa^{-1} at 1 kPa, thus bridging the gap in low-pressure performance. This thesis addresses this limitation by demonstrating a hollow nanofiber dielectric system capable of maintaining linear behaviour and mechanical stability across a wide pressure ranging up to 300 kPa, verified through multi-level cyclic loading. Although coaxial electrospinning is known in other fields, its application for engineering dielectric layers in capacitive sensors remains rare. The potential of hollow structures for enhancing compressibility and sensitivity is underutilized.
The use of hollow PCL nanofibers as a dielectric medium, demonstrates the capability of internal architecture to tune dielectric response and improve sensor performance in low-pressure conditions. This work also studied a new perspective by conducting a direct head-to-head comparison between control and hollow fiber-based sensors, fabricated from the same polymer i.e., PCL and characterized identical experimental setups. The results highlight around 90% enhancement in low-pressure sensitivity for hollow fibers.

3 Materials and Methods

3.1 Materials

For electrospinning procedure, Polycaprolactone (PCL) was purchased from Sigma-Aldrich (Mw ≈ 50,000). Dichloromethane (DCM) and N, N-dimethylformamide (DMF) was used from Sigma-Aldrich, served as the solvent system for electrospinning. A silicone oil (polydimethylsiloxane) was utilized as the core fluid for coaxial electrospinning. This oil was later removed to create the hollow fiber structure. Flexible indium tin oxide (ITO) on PET substrates (ITO-coated PET) was used from Sigma Aldrich were used as the electrode films. Each ITO/PET sheet was cut to 1.5 × 3 cm^2 to define the sensor area. Standard transparent cellulose tape (3M) was used to encapsulate the sensor assembly. Copper connecting wires was used to provide electrical connections to the ITO electrodes. Diethyl ether was used as a solvent to extract the silicone oil core from fibers. Polyvinyl alcohol (PVA) (Mw ~89,000, Sigma-Aldrich) was prepared as a 2 wt% aqueous solution for core for assisting cross-section preparation for SEM analysis. All materials were used as received without further purification. Solutions were prepared using deionized water and analytical-grade solvents as needed.

3.2 Electrospinning Procedure

Electrospinning was employed to fabricate both control nanofibers and coaxial nanofibers. Electrospinning apparatus (Spinbox® by Bioinicia, Spain) was used for all experiments. The electrospinning environment was maintained at ~22 °C under ambient humidity. Fibers were collected on a grounded aluminium foil attached to a flat collector plate.

3.2.1 Single-Shell Nanofiber Preparation (Control)

For control PCL nanofibers, a 12 wt% PCL solution was prepared by dissolving PCL in a 1:1 DCM/DMF solvent mixture. The polymer solution was magnetically stirred at 160 rpm overnight at room temperature to ensure complete dissolution and homogeneity. This solution was loaded into a 10 mL plastic syringe fitted to the electrospinning pump. The electrospinning conditions were adjusted to obtain uniform fibers without beads. A positive voltage of 15 kV was applied to the needle tip, and the solution was fed at a flow rate of 1.67 µL/min. The tip-to-collector distance was set to 10 cm. Under these conditions, a stable Taylor cone and fluid jet were maintained which produce smooth PCL fibers. The fibers were collected as a non-woven mat on the aluminium foil collector. Each mat is produced after 5 minutes of

electrospinning to ensure uniform thickness and uniformity across the mat. The resulting control PCL nanofiber mat was carefully peeled off from the foil and placed onto a clean glass slide for handling and characterisation.

3.2.2 Coaxial Nanofiber Preparation

For coaxial electrospinning (core–shell fiber fabrication), a two-fluid setup was used with two syringes operating simultaneously. The sheath solution consisted of 12 wt% PCL solution in a solvent ratio of DCM/DMF = 4:1. The high concentration of DCM enables fast evaporation rate which enables smooth formation of peelable fibers from the collector plate. This PCL solution was stirred at 160 rpm overnight and then loaded into a 10 mL syringe connected to the sheath needle of a coaxial spinneret. Silicone oil was used as the core material. It was loaded into a separate 10 mL syringe feeding the inner needle. The coaxial needle assembly had an inner needle diameter of 0.6 mm and an outer needle inner-diameter of 1.4 mm, creating a concentric core-shell ejection geometry.

During coaxial electrospinning, the PCL sheath solution and silicone oil core were pumped simultaneously at optimized flow rates of 22 μL/min for the sheath solution and 8 μL/min for the core. A positive voltage of 15.5 kV was applied to the coaxial needle, and a TCD of 15 cm was maintained. These parameters were found to produce a stable coaxial jet and prevent premature breakup of the core. Fibers were collected on aluminium foil as a random mat, similar to the single-fiber case. All electrospinning runs were performed under consistent ambient conditions (~22 °C) The coaxial nanofiber mat, having liquid silicone oil, was allowed to dry briefly on the foil, then carefully peeled off and transferred onto a glass slide for support.

3.2.3 Post Processing of Hollow Fibers

To obtain hollow fibers, the silicone oil core was removed by a solvent extraction method. The as-spun coaxial fiber mat was immersed in diethyl ether, which acts as a good solvent for the silicone oil but a nonsolvent for PCL. The mat was soaked in diethyl ether twice, first for 15 minutes, then in fresh diethyl ether for an additional 30 minutes. This sequential soaking ensured complete dissolution and leaching out of the silicone oil from the core. During this process, the fiber mat was kept stationary to avoid mechanical disturbance. After extraction, the mat was gently removed and placed in a ventilated hot plate at 45 °C for 1 hour to evaporate residual ether and dry the scaffold. The successful removal of the core oil yields hollow PCL

nanofibers, which have an empty channel. The dried hollow fiber mats were stored in a clean, desiccated environment prior to device assembly and characterisation.

3.3 Morphological Characterisation

3.3.1 Optical Microscopy

Initially, the morphology of the electrospun fibers was examined using an optical microscope (Euromex Microscopes iScope) to confirm fiber formation and uniformity. Small sections of the fiber mats were placed on glass slides and observed under bright field illumination at 20X, 40X, and 70X magnifications. Optical images verified the presence of continuous fibers without significant beading or agglomeration. This quick optical inspection ensured that the electrospinning parameters were yielding fibers as intended, prior to more detailed microscopic analysis.

3.3.2 Scanning Electron Microscopy

For high resolution imaging, the fiber samples were analysed by scanning electron microscopy (Thermo Scientific Inc., Eindhoven, NL) at an accelerating voltage of 2 kV and a beam current of 25 pA. These low-voltage conditions were used to minimize charging on the non-conductive PCL fibers. Prior to SEM, platinum sputtering was performed on the fibers mat to produce conductive coating. Fiber mats (both control and hollow) were mounted on aluminium SEM stubs using carbon adhesive tape. To visualize the surface morphology, top view SEM micrographs were taken at various magnifications. Hollow fibers were expected to show a slightly larger diameter and possibly a contrast between core and shell regions.

3.3.3 Cross-Section Preparation

In order to visualize the hollow interior of the coaxial fibers, cross-sectional samples were prepared with 2 wt% PVA as core. The PVA infiltration is easier to remove, being dissolvable in water, for cross-section analysis. Further, it also helped to preserve the fiber structure during sectioning. Then, a focused ion beam or broad ion beam milling step was employed at cryogenic temperatures (cryo-ion milling) to produce a clean, smooth cross-sectional surface through the fibers. Cross-section on the electrospun fibers were prepared using broad argon ion beam mill (ArBlade 5000, Hitachi High-Technologies, see Figure 10) with an acceleration voltage of 3.5 kV. In order to limit possible thermal effects on the polymers, the sample was kept at 40 ^{o}C during the milling. This process removed any smeared polymer and revealed the core–shell

structure clearly. The cross-section was then observed in the SEM, where the hollow core of the fibers could be identified as a distinct internal void or a contrast difference (due to the PVA fill, which appears darker). This combined approach ensured that the true hollow structure (core diameter and shell thickness) could be visualized without significant collapse of the fibers.

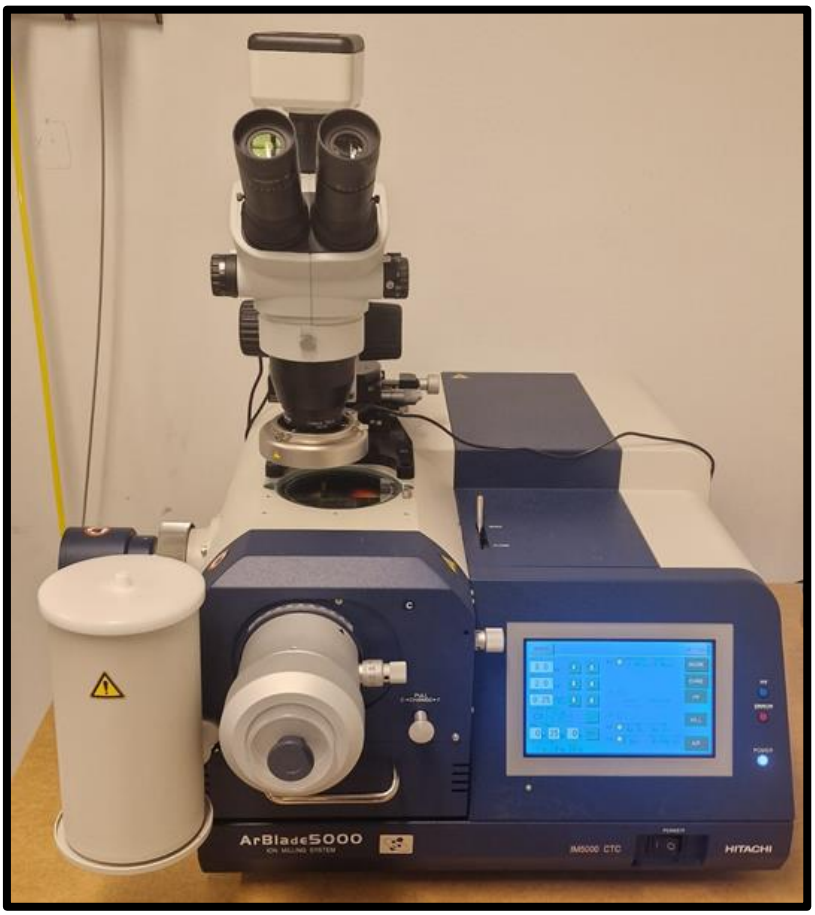

Figure 10 shows image of Ion Milling Setup (ArBlade 5000, Hitachi High-Technologies) available in Quantum building, University of Turku.

3.4 Device Fabrication

Flexible capacitive pressure sensor devices were fabricated by integrating the electrospun fiber mats as the dielectric layer between two flexible ITO electrodes. The detailed stepwise fabrication process (as shown in Figure 11) is mentioned below;

- Fresh ITO coated PET films (each 1.5 × 3 cm^2) were used as the top and bottom electrodes.

- Before assembly, protective layers were carefully removed and the ITO surfaces were cleaned with isopropanol to ensure optimal electrical contact. The electrodes were handled such that their conductive sides faced inward in the final sensor configuration.

A section of the electrospun PCL nanofiber mat (control fibers or the hollow core post processed by oil extraction) was trimmed to match the electrode dimensions and positioned over one of the ITO films, fully covering its active area. This fiber mat functioned as the dielectric mat in the capacitive structure.

- The second ITO/PET electrode was then aligned on top of the dielectric layer with its conductive side oriented downward, creating a sandwich configuration. Particular care was taken to ensure full overlap and proper alignment of the electrodes to define a consistent capacitance area.

- To stabilize the structure, the stack was gently pressed and encapsulated using transparent cellulose tape applied around the active region. This lamination step not only fixed the dielectric layer in place but also provided mechanical support while maintaining the flexibility.

- A portion of each ITO electrode was left exposed at one end to allow electrical connection. Copper wires were attached to the exposed ITO ends, one per electrode, using carbon tape. The connections were further reinforced with tape to prevent delamination. The assembled device thus formed a flexible parallel-plate capacitor with an effective sensing area of approximately 4.5 cm^2. The overall device thickness consisted of two ITO/PET substrates. All fabricated sensors were visually inspected to verify uniform layer stacking, absence of air gaps, and integrity of the encapsulation.

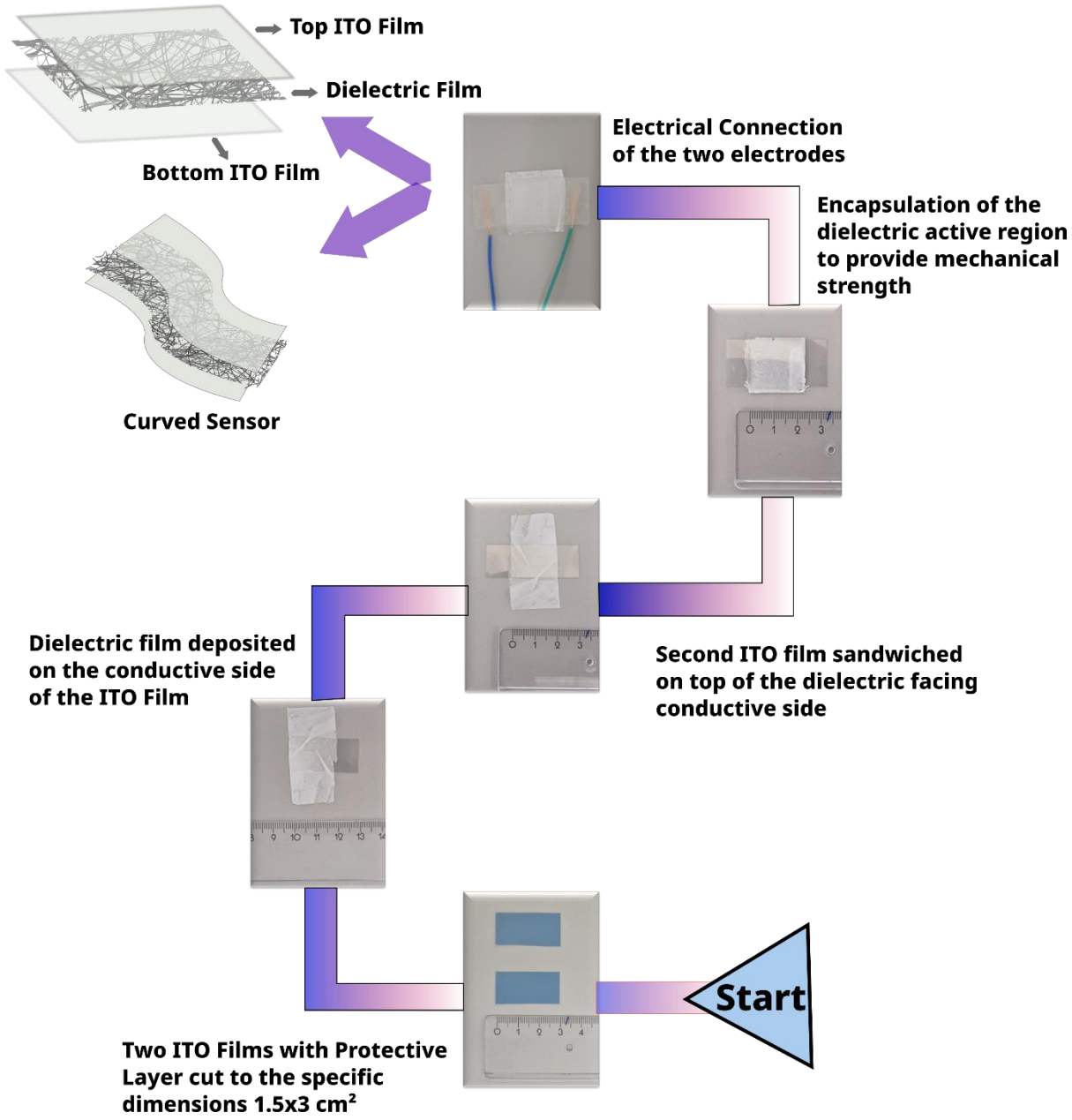

Figure 11 shows Flow diagram of fabrication process along with schematic of fabricated sensor.

3.5 Electrical Characterisation

The pressure sensing performance of the devices was evaluated by measuring their capacitance response under applied pressure. A Texture Analyzer TA (Model TA.XT. plus100C, Stable Micro Systems, UK) was used to apply compressive force to the sensor, while a precision LCR (Inductance, Capacitance, Resistance) meter (GW Instek LCR-6300) simultaneously measured the device capacitance as shown in Figure 10a. The sensor was placed on the base platform of the texture analyzer, and a flat-ended cylindrical indenter (10 mm diameter) was mounted to

the moving head of the analyzer (see Figure 10b). This indenter area (78.5 mm^2) defined the contact area for pressure application. The TA was programmed to move the indenter vertically and to press against the sensor with controlled displacement or force. The LCR meter was connected to the sensor leads to record capacitance in real-time during mechanical testing. The LCR meter was configured in continuous measurement mode, and its output (capacitance in Picofarads) was read by a computer throughout the test. A custom MATLAB script was interfaced with the LCR meter, allowing synchronized data acquisition of the capacitance while the TA applied the load.

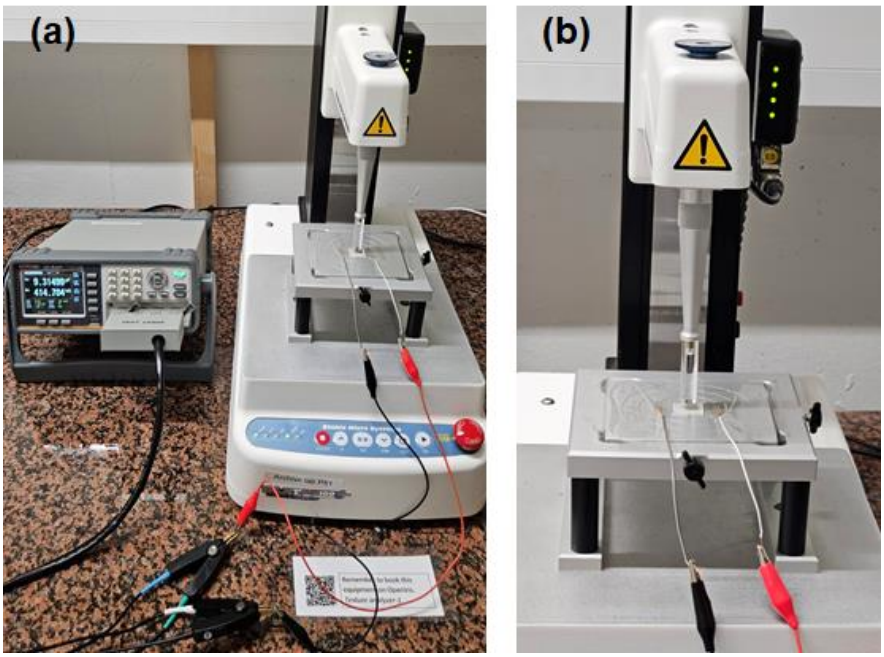

Figure 12 (a) shows Texture Analyzer (TA) setup connected with LCR (b) shows closed view of TA cylinder facing the sensor.

4 Results and Discussion

4.1 Schematic Overview

The overall fabrication and sensor integration process is illustrated schematically in Figure 13. The process begins with the preparation of a polymer solution for coaxial electrospinning. PCL is dissolved in a solvent mixture and loaded into a syringe as the sheath solution, while a core (silicone oil) is loaded into a syringe as the core. A high-voltage is applied, which produces a core–shell jet that solidifies into continuous fibers with a PCL shell and a liquid core. Diethyl ether is then used to remove the liquid core, leaving behind hollow PCL nanofibers (with air-filled cores) The resulting hollow fiber mat is dried and subsequently assembled into a capacitive sensor by sandwiching it between two flexible ITO electrodes on PET substrates. The layered structure is encapsulated (e.g., with thin tape), and electrical leads are attached to the ITO, fabricating a flexible capacitive pressure sensor device.

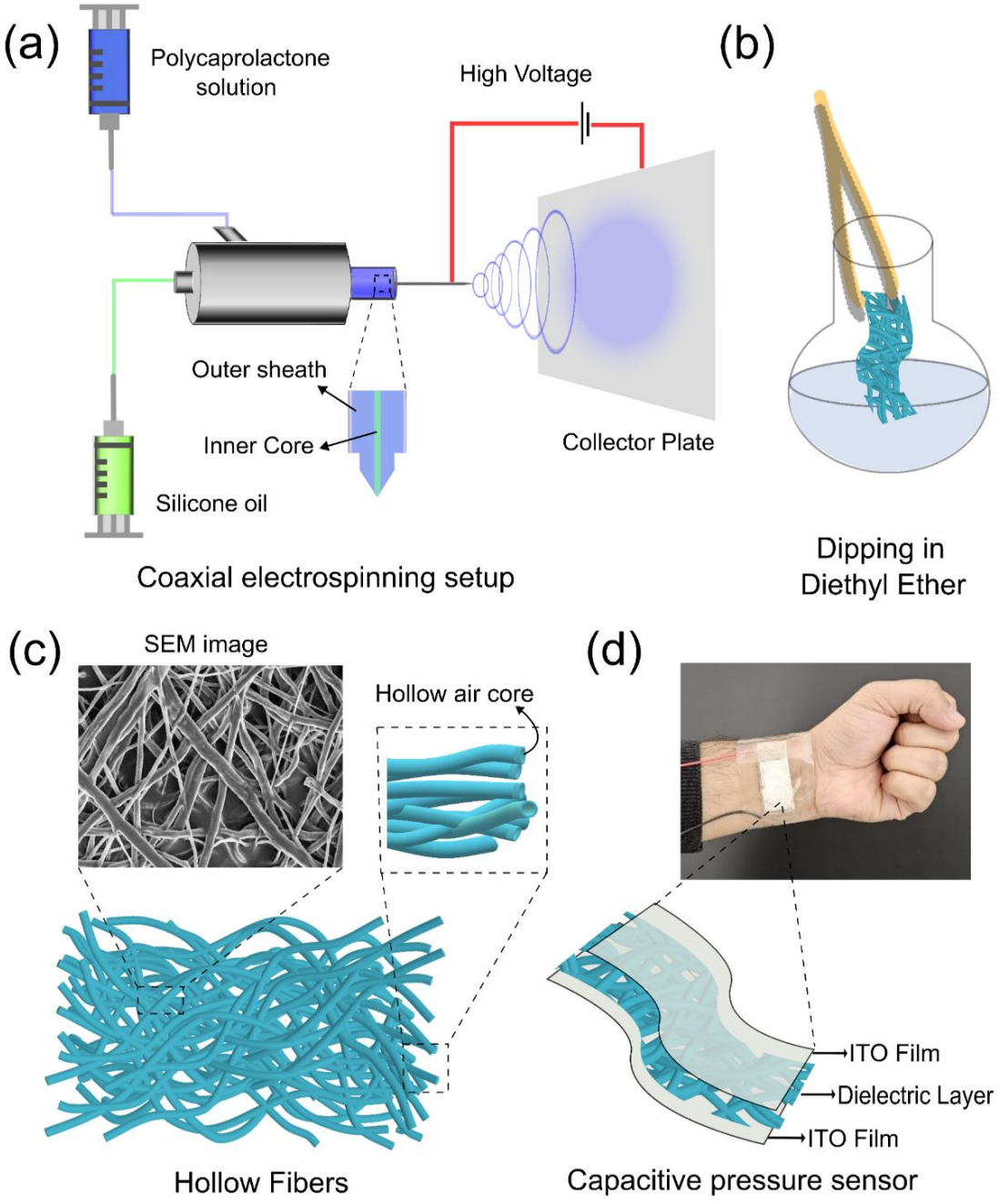

Figure 13 (a) shows coaxial electrospinning setup for core–shell fiber production. (b) shows removal of the silicone oil core by immersion in solvent, yielding hollow fibers. (c) SEM image of the coaxial fibers after core removal and schematic of a hollow fiber mat. (d) demonstrating the integration of sensor to the skin [44].

4.2 Microscopy and Morphology

Optical microscopy was used as an initial assessment of fiber formation for both the hollow and control nanofiber mats. Both types of electrospun fiber mats appear as uniform, non-woven films without obvious defects or bead formation. The fibers are distributed randomly, forming

a porous network. Both the hollow fiber mat and the control fiber mat exhibit a white, translucent appearance under the optical microscope, indicating successful deposition of a continuous. No large agglomerates or inconsistencies are seen in either sample, suggesting that the electrospinning conditions produced homogeneous mats in both cases. Although the optical microscope cannot directly show the internal hollow core, the hollow fibers often exhibit a subtle variation in contrast along their cross-section, potentially due to light scattering from their core–shell structure. In contrast, the control fibers appear as solid opaque strands with uniform brightness. Importantly, no beads or discontinuities are observed for either fiber type, indicating good electrospinning stability and fiber uniformity as depicted in Figure 14.

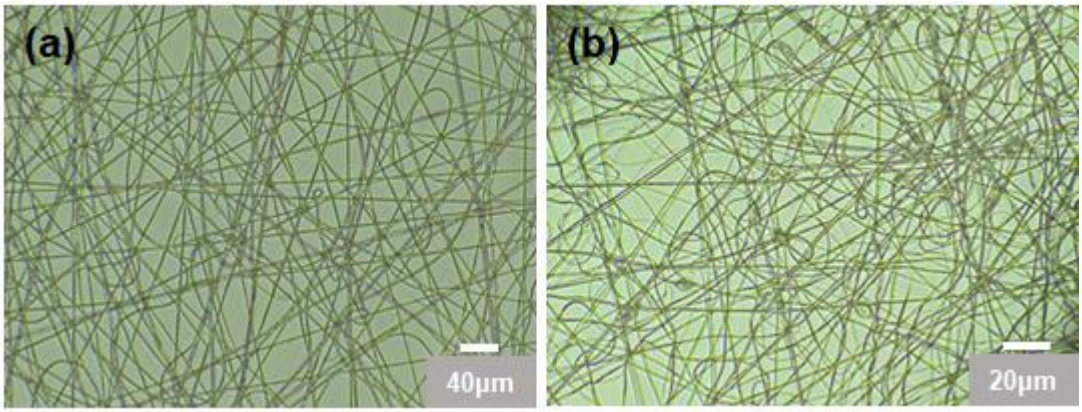

Figure 14 (a) shows Optical Images of Control nanofibers which appear as solid opaque strands with uniform brightness (b) shows Coaxial nanofibers with contrasting core-shell structure due to light scattering.

High resolution SEM was used to examine the fiber morphology and cross-sectional view of coaxial fibers. Figure 15 (a) and (b) shows representative SEM images of the coaxial nanofibers and the control nanofibers. At 100 µm, the hollow PCL fibers form a uniform, bead-free mat of fibers. The fibers have relatively smooth surfaces and consistent shape along their length, indicating stable jet formation during coaxial electrospinning. Similarly, the control PCL fibers, produced by single nozzle electrospinning, also form a uniform non-woven mat with no beads. The control fibers are visibly thinner in diameter than the hollow fibers. Both samples show a high degree of porosity due to the spaces between fibers. The uniform deposition of fibers across the substrate is evident in both cases, confirming reproducible fabrication. At higher SEM magnifications, the hollow fibers occasionally show minor surface roughness or tiny groove-like defects on the fiber surface, whereas the control fibers generally appear smooth. These small surface features on the hollow fibers may result from the coaxial process or rapid solvent evaporation however, they do not show large beads. Overall, the SEM images verify

that both the hollow and solid fibers were successfully produced with good uniformity, and that the primary difference lies in their diameter and internal structure.

A cross-sectional view of ion milled hollow fiber clearly reveals a lighter outer ring and a darker interior. This contrast arises because the polymer shell (PCL) scatters electrons differently than the air-filled core, resulting in a bright ring (shell) surrounding a darker centre in the SEM image. The distinct core region inside the fiber is direct evidence that the silicone oil was successfully removed, leaving an empty lumen. Most hollow fibers exhibit this clear core–shell morphology, although the core diameter can vary from fiber to fiber. The hollow fibers also tend to have larger overall diameters than the control fibers, consistent with the coaxial nozzle producing a thicker fiber to accommodate the core. These SEM observations align with the optical microscopy impressions and provide definitive visualization of the hollow interior in the coaxial fibers. Minor flattening of fibers is sometimes observed in hollow fibers when imaged under SEM vacuum. This can be explained as the soft PCL can be compressed by the substrate or while handling. However, the overall cylindrical shape and hollow nature are preserved in the images.

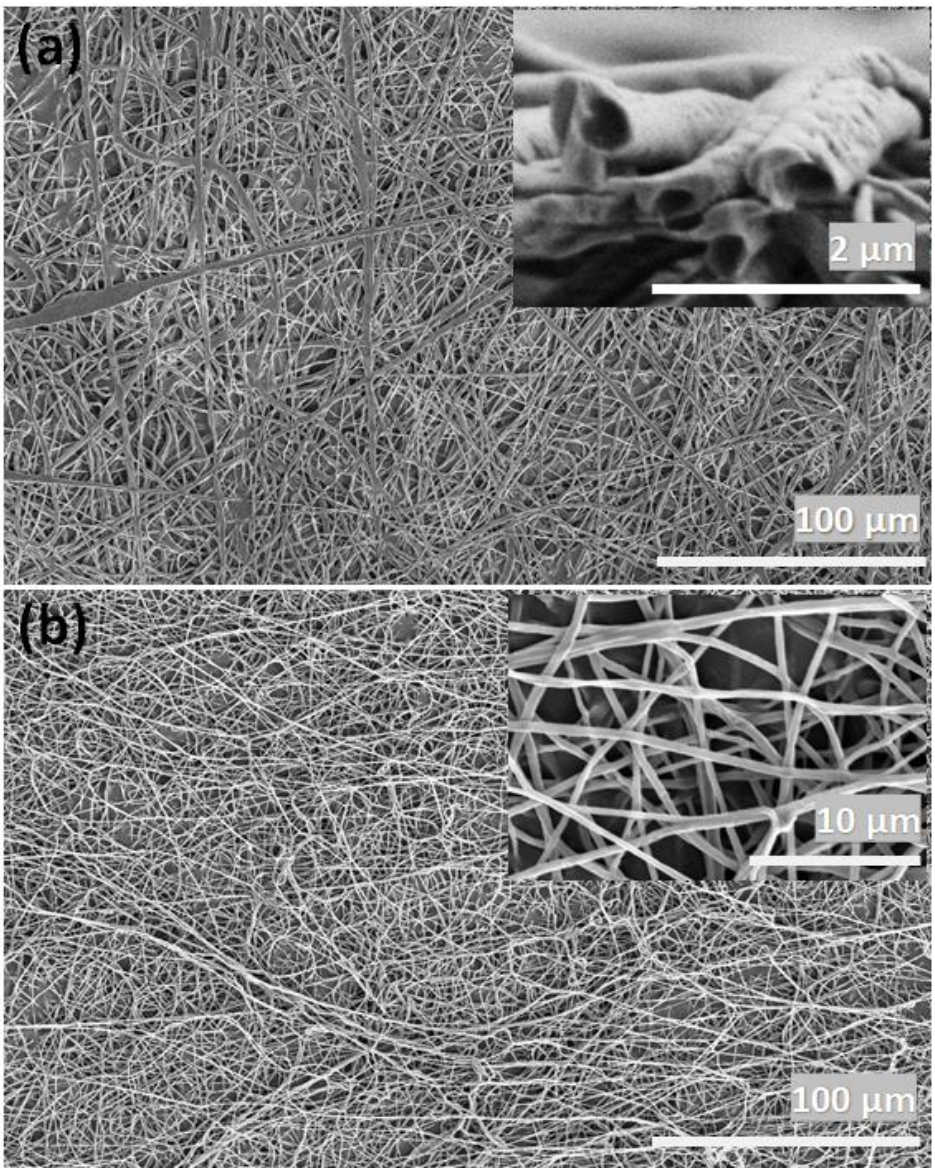

Figure 15 (a) shows Scanning Electron Microscopy (SEM) images of Coaxial fibers. Inset: Cross-sectional view of the hollow fibers (b) shows Control PCL fibers. Inset: Magnified image of Control fibers.

4.3 ImageJ Analysis

Image J is used to study the diameter distribution for both types of fibers (as seen in Figure 16) and the quantitative results are summarized in the Table 2. The average fiber diameter of the hollow fibers was measured to be about 0.89 µm, which is roughly double the average diameter of the control fibers i.e., ~0.43 µm. The distribution of diameters for the hollow fibers is relatively broad. While many hollow fibers are around 0.8–1.0 µm in diameter, some fibers were as thick as approximately 2 µm. In contrast, the control fibers had a much narrower size distribution, with most fibers in the few hundred nanometre range and 0.6 µm at the thickest. This significant size difference reflects the presence of the core in the coaxial process, which

inflates the fiber diameter. Such diameter values are in line with typical electrospun nanofiber dimensions (electrospun fiber diameters generally range from tens of nanometres up to a few micrometres depending on processing conditions)

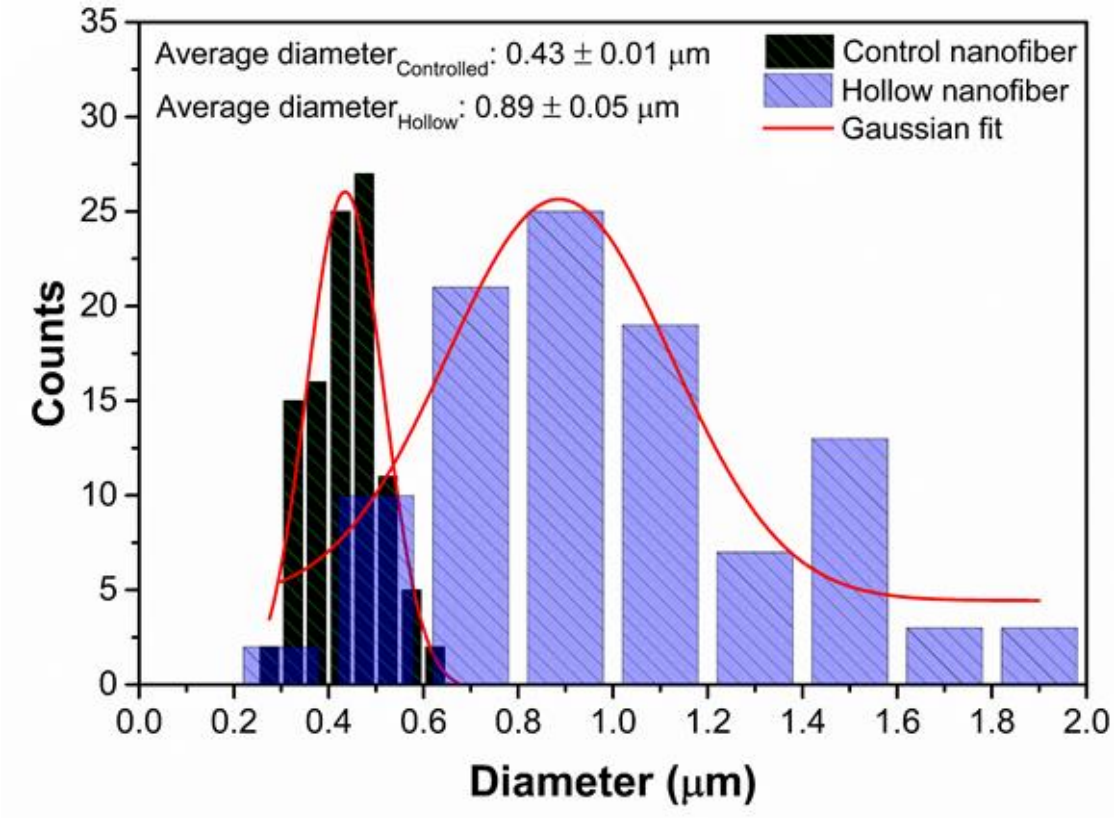

Figure 16 shows diameter distribution of Control and Coaxial fibers analysed by Image J. It shows the average diameter of the control fibers around 0.43 µm and for coaxial fibers around 0.89 µm.

In addition to fiber diameter distribution, the ImageJ analysis and cross-sectional SEM images was used to measure the core and sheath thickness of coaxial fibers along with porosity of both the fibers. The hollow fibers represents an internal void roughly on the order of 0.8 µm in diameter and a PCL shell thickness of only about 0.047 ± 0.002 µm on each side. This extremely thin shell suggests that the majority of the fiber's cross-section is empty air, which is consistent with the goal of maximizing the air content in the dielectric. It should be noted that not every fiber had a perfectly uniform core. Some variation in core diameter and shell thickness was observed indicating slight fluctuations in the coaxial jet during fabrication. Nonetheless, the average values above were reproducible across multiple fibers. The porosity of the fibrous mats was also evaluated. The hollow fiber mat was found to have a porosity of approximately 29.7%, while the control fiber mat had a slightly higher porosity of around 35.7%. This somewhat lower porosity in the hollow fiber mat is attributed to its thicker fibers (fewer fibers per unit area) Table 2 collates these key morphological parameters side by side for hollow and control

fibers, serving as a convenient reference for subsequent discussions on how these structural differences impact sensor performance.

Table 2 shows comparison of morphological parameters of hollow and control fibers.

Morphological Parameters	Fiber diameter	Shell thickness	Porosity	Morphology	Surface area	Fabrication complexity
Hollow fibers	0.89 µm	0.047 ± 0.002 µm	29.74%	Core-shell/hollow structure	Higher to hollow core	Higher, due to coaxial setup
Control fibers	0.43 µm	no	35.73%	solid cylindrical structure	Lower	Lower, due to single nozzle setup

4.4 Sensitivity Analysis

The sensitivity of the capacitive sensor was measured across a broad range of applied pressures. However, particular attention is given to the low-pressures. Figure 17 summarizes the relative capacitance change ($\Delta C/C_o$) as a function of pressure. In the low-pressure range i.e., 0.2–2 kPa, the hollow fiber-based sensor exhibits a steep increase in $\Delta C/C_o$ even for small increments in pressure. The device is able to detect pressures as low as 0.2 kPa, producing a measurable capacitance change at that minimal load. The slope of the $\Delta C/C_o$ versus pressure curve in this initial region corresponds to a sensitivity of approximately 1.05 kPa^{-1} at 1 kPa for the hollow fiber sensor. Indeed, the sensor sensitivity at 0–2 kPa outperforms many prior nanostructured dielectric sensors (discussed in the Literature Review). The high sensitivity is attributed to the hollow fiber dielectric i.e., under low loads, the thin walled fibers and trapped air voids deform significantly, causing high sensitivity. In practical terms, this means the sensor can detect very slight touches or gentle pressure fluctuations. We also note that the response in low-pressure loading is fairly linear up to around 1–2 kPa, after which the curve begins to bend as it enters the transition to higher pressures. Such linearity at low-pressure is advantageous for quantitative sensing of subtle forces.

At higher pressures, the hollow fiber sensor transitioned towards saturated response and the sensitivity decreases. Beyond roughly 2–5 kPa, the curve flattens considerably. The initially steep slope cannot be maintained as pressure increases. It is owing to the dielectric layer air gaps and fiber compressibility become saturated. At tens of kilo pascals, the hollow fiber mat has been significantly compacted. Consequently, the hollow cores are largely collapsed and the fibers are densely pressed together. In this state, additional pressure causes relatively smaller

changes in the capacitance due to the inherent porosity of the polymer. Thus, the sensitivity drops at higher pressures, eventually falling below the sensitivity that a conventional solid fiber sensor shows in that range. In quantitative terms, while the hollow fiber sensor had 1.05 kPa^{-1} sensitivity around 1 kPa and when pressure is applied in the 50–100 kPa range, its slope is much lower 0.01–0.02 kPa^{-1}, depicted in Figure 17. In fact, the maximum sensitivity of the hollow fiber sensor occurs at 1 kPa and then continuously decreases with pressure.

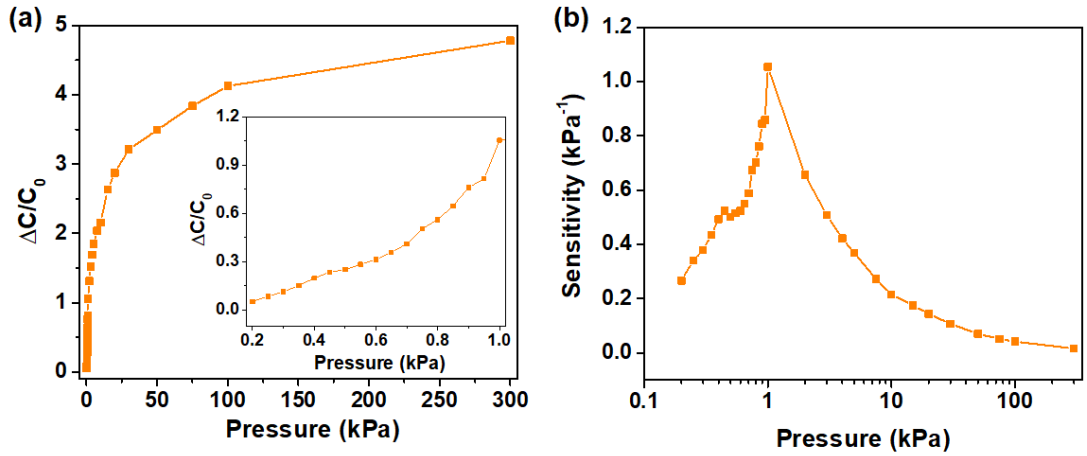

Figure 17 (a) shows relative capacitance plotted as a function of pressure. Inset shows the magnified graph for lower pressure range. (b) Sensitivity of the pressure sensor as a function of pressure.

A comparative analysis of hollow and control nanofiber is employed based on their sensitivity (see Figure 18) Both sensors were fabricated on the same ITO electrode platform, and both were tested under the same conditions. On the other hand, control sensor reaches its peak sensitivity at a higher pressure and then plateau. The maximum sensitivity of the control sensor was measured to be about 0.54 kPa^{-1} and occurred at a relatively higher pressure at 5 kPa. This peak sensitivity of the control is approximately half that of the hollow fiber sensor's peak i.e., 1.05 kPa^{-1} at 1 kPa. Beyond roughly 4–5 kPa, the control sensor exhibits a more linear and sustained increase in capacitance, while the hollow sensor curve is flattening out. This difference means that in the high-pressure regime, the incremental response of the coaxial fiber sensor is actually less than that of the control sensor. The reason behind that at higher pressure, the hollow structure has fully collapsed under pressure and the dielectric layer behaves more like a solid film (losing the advantage of the internal air). The compressibility gets saturated and the device stiffness increases and further pressure yields diminishing capacitance change. Therefore, there is a trade-off in sensor performance i.e., extremely high sensitivity in the low-pressure regime, at the cost of reduced sensitivity in the high-pressure regime. The consistent

performance in this regime is evident from the error bars being small and the sensor response being reproducible over multiple trials. This behaviour is actually desirable for many targeted applications (e.g., touch or pulse sensors need high gain at low-pressure and can tolerate lower gain at high force, which might even protect the sensor from overload. These findings validate our design strategy for low-pressure sensing, while also highlighting the inherent limitation of the hollow structure under heavy loads.

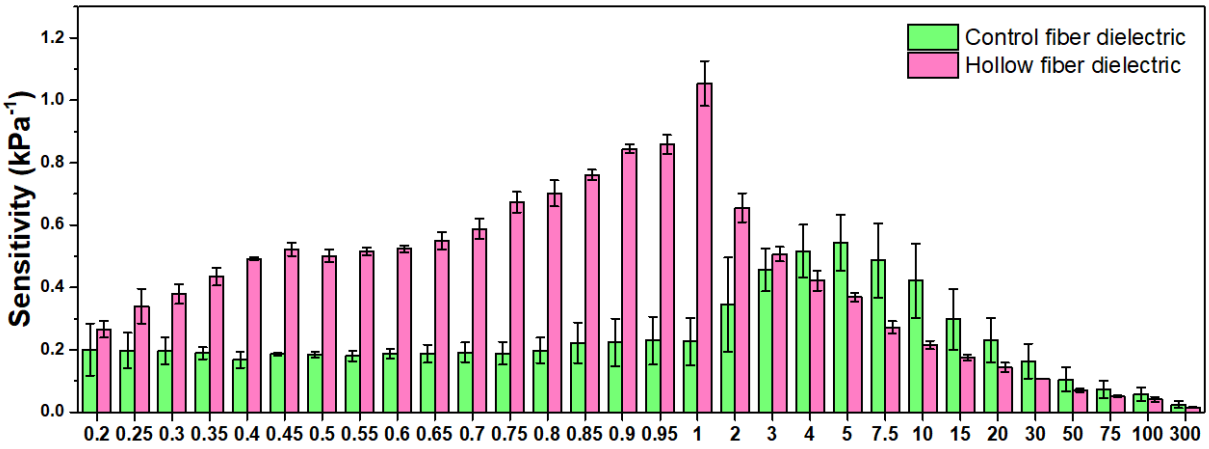

Figure 18 shows comparison of the sensitivity of the pressure sensor produced with hollow nanofibers and control nanofibers of PCL. The histogram peaks represent the average sensitivity and error bars show the standard deviation.

4.5 Cyclic Testing and Durability

Cyclic pressure tests have been conducted on the hollow fiber sensor to demonstrate its viability in practical applications monitoring $\Delta C/C_o$ response over 1000 repeated cycles at various pressure levels. The results in Figure 19 (a-d) indicate excellent stability and durability of the device. At a low-pressure of 1 kPa, the change in capacitance over initial capacitance remained highly consistent over 1000 cycles, with negligible baseline drift or signal attenuation. The peaks increased and returned to baseline with each loading/unloading in a virtually identical manner, demonstrating that the hollow fibers elastically recover their shape after each pressure release. The relative change in capacitance for 1000 cycles test shows only 8% deviation from average reference peak, indicating minimal signal drift. This suggests that the PCL hollow fiber dielectric does not undergo significant plastic deformation or fatigue under repeated small stresses hence, yielding reproducible capacitance.

Similar testing has been performed at 10 kPa, 100 kPa, and 300 kPa, respectively as shown in Figure 19 (b-d). In all cases, the sensor was able to withstand the cyclic loading without mechanical failure or delamination, and the capacitance response remained consistent. At 10

kPa, the hollow fiber sensor again showed steady and repeatable capacitance peaks for each cycle with minimal signal drift over 1000 cycles. At 100 kPa and even at the extreme pressure of 300 kPa, the device continued to function reliably throughout the cycles. The overall trend was that no significant degradation occurred, the sensor signal in cycle 1000 was virtually the same as in cycle 1 at each tested pressure with minimal signal drift.

The hollow fiber dielectric thus exhibits excellent mechanical resilience, absorbing and releasing even at large pressures repeatedly while maintaining its structural integrity. This resilience can be attributed to the intrinsic elasticity of PCL and the air-filled structure upon unloading. Even though individual fibers may appear somewhat flattened after high-pressure cycling (when observed under SEM post-test), the fibrous network as a whole recover sufficiently to give consistent electrical readings. The cyclic testing confirms that the sensor is reliable for long-term use and does not suffer from early fatigue or hysteresis build-up. The stable cyclic performance at pressures spanning 1 kPa to 300 kPa also indicates that the device can be used in a wide range of scenarios (from gentle physiological pressures to heavy touches) without needing recalibration frequently. In conclusion, the hollow nanofiber pressure sensor demonstrated outstanding durability in repetitive loading, reinforcing its suitability for real world applications where sensors may undergo thousands of cycles.

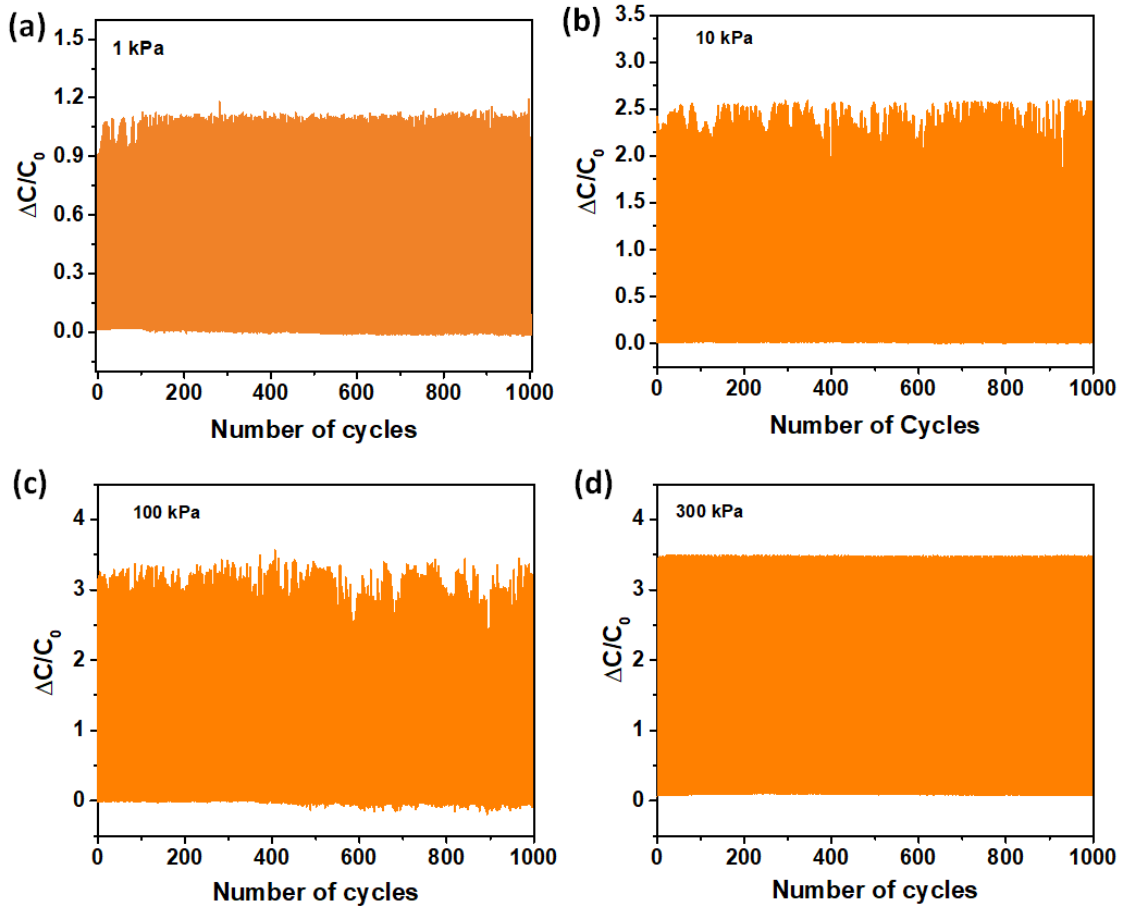

Figure 19 shows relative change in capacitance at different pressures i.e., (a) 1 kPa, (b) 10 kPa, (c) 100 kPa and (d) 300 kPa of Coaxial Fibers.

4.6 Response and Recovery Time

The transient behaviour of the hollow fiber sensor is characterised by applying stepwise-pressure inputs and measuring the time dependent capacitance change. In a representative test, a pressure of 1 kPa was rapidly applied and held for 10 seconds, then released, while recording the sensor output (see Figure 20a). The capacitance rose to a steady value with a measured response time of approximately 84 ms, defined as the time to reach 90% of the full ΔC after the pressure was applied. When the pressure was removed, the capacitance similarly decayed back to baseline with a recovery time of around 162 ms. These sub-0.2 second response and relaxation times indicate that the sensor is quite fast, easily capable of tracking human physiological events (which often occur on timescales of fractions of a second or longer). The transient curves in Figure 20 (b) & (c) show a sharp initial change and then a smooth plateau, with no overshoot or oscillation, suggesting the sensor's response is stable. However, it is also observed that the recovery is a bit slower than the response. This kind of response is common

in polymeric sensors as the material and structure take slightly longer to fully rebound than to compress. The transient performance was found to depend on factors such as the applied pressure level and the speed at which the pressure is applied. For instance, at higher pressures the response time can sometimes be shorter because a larger force accelerates the deformation. While at very slow loading rates the effective measured response time can appear longer since the stimulus itself is gradual. To systematically evaluate this, we performed additional tests varying the pressure amplitude and the loading speed in Figure 20 (d) & (e). The results confirmed that both response and recovery times stay on the order of tens to a couple of hundred milliseconds across various conditions. Also, faster loading tends to produce faster responses, whereas heavy pressures can sometimes slightly prolong the recovery due to the greater deformation needing to relax.

Comparing the sensor dynamic response to literature, it is competitive with the state-of-the-art flexible pressure sensors. Many recent nanostructured or micro structured capacitive sensors report response times in the range of 10–100 ms, which comes under the bracket of 84 ms response of our device. For example, a wearable sensor using electrospun polyvinylpyrrolidone (PVP) nanofibers achieved a rapid 41 ms response and 36 ms recovery, reflecting the naturally fast elasticity of nanofiber mats [59]. Another work employing a graphene aerogel dielectric showed an impressively fast 50 ms response, though its recovery was much slower i.e., around 230 ms, due to the internal damping in the aerogel structure [60]. In our case, the 162 ms recovery falls in between these examples i.e., slower than the very fastest nanofiber sensors but faster than some other designs that involve viscoelastic materials or air trapping. Meanwhile, some highly sensitive sensors using thicker polymer structures have response times exceeding 150 ms, indicating that our device is at least as quick or quicker than those. It is encouraging that despite the relatively soft and highly porous nature of our dielectric layer, the response speed is not significantly compromised.

Thin PCL shells and the microscopic length scale actually allow the hollow fibers to deform rapidly with minimal viscous lag. The sensor response time, i.e., 0.08 s, is more than sufficient for detecting normal human activities such as pulse rate and speaking vibrations which typically occur on timescales of 0.1–1 s, and even fast events like object impact or typing (~10–50 Hz events) can be captured. The recovery time of 0.16 s, being slightly longer still permits a potential bandwidth of several Hz, suitable for many real-time monitoring tasks. In conclusion, the transient characterisation shows that the hollow nanofiber sensor can quickly respond to pressure changes and reset to baseline, with performance comparable to other high-sensitivity

flexible sensors in the literature. There is room for future optimization by reducing recovery time. This can be possible by material tweaks or nano structuring techniques discussed in the literature review. However as-built, the device performance is adequate for its intended applications.

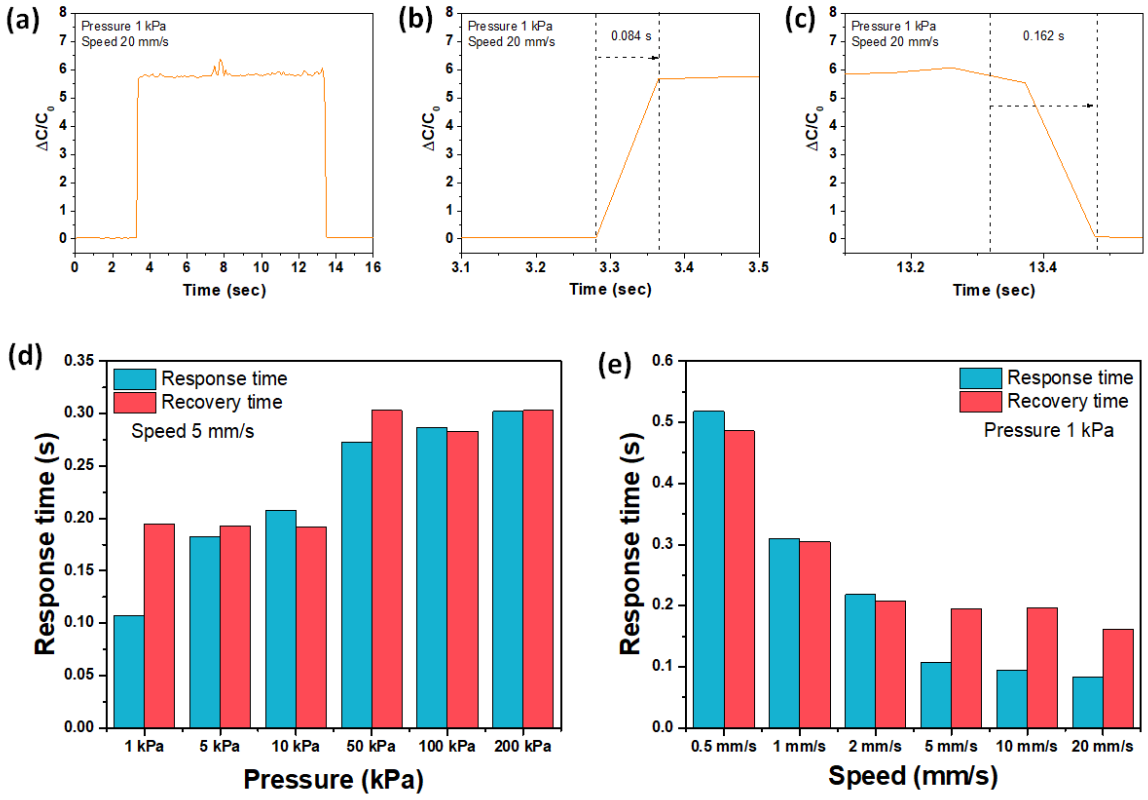

Figure 20 (a) shows step-wise response of sensor at 1kPa. (b) shows response time at 1kPa. (c) shows recovery time at 1kPa. (d) and (e) shows trend of response and recovery w.r.t pressure and speed respectively.

4.7 Performance Comparison with Reported Flexible Sensors

To contextualize the performance of hollow nanofiber capacitive sensor, a comparative table is drawn with other recently reported flexible pressure sensors (see Table 3 for an overview of key metrics). In terms of sensitivity, our sensor showing maximum sensitivity of 1.05 kPa^{-1} in low-pressure range, is among the highest reported for low-pressure flexible sensors. Many flexible capacitive sensors using planar or less-structured dielectrics have sensitivities well below 1 kPa^{-1}. For instance, biodegradable plant leaf-based sensors were demonstrated with natural skeletons as dielectrics but their sensitivities were only on the order of 0.08 kPa^{-1} or even lower. Another work using a rubberized leaf skeleton reported a sensitivity of just 4.5×10^{-3} kPa^{-1}. These natural material sensors prioritized eco-friendliness but clearly trade-off

sensitivity. Approaches that introduce microstructures in elastomeric dielectrics fare better. A cylindrical ladder micro structured PDMS sensor showed 0.12 kPa^{-1} sensitivity, and a "cheetah leg" inspired 3D microstructure achieved about 0.75 kPa^{-1} sensitivity. While 0.75 kP^{-1} is quite respectable, it is still about 30% lower than our hollow fiber sensor's peak sensitivity. Only a few designs have reported sensitivities on the order of 1 kPa^{-1} or above. One example is a sensor with an aligned airgap dielectric with an array of sealed air cavities which reached 1.277 kPa^{-1}. Another notable example is a device using an electrospun PI nanofiber membrane as dielectric, which attained a very high sensitivity of 2.2 kPa^{-1}. However, that device required additional micro structuring and was tested primarily in a relatively high-pressure regime (it could handle up to 1.4 MPa). In summary, against the landscape of flexible sensors, our hollow PCL fiber sensor ranks at the top tier of sensitivity for the low-pressure region, exceeded only by a couple of recently developed devices that either involve more complex fabrication or different material systems. This work has achieved high sensitivity using a simple, scalable fabrication (coaxial electrospinning and straightforward assembly) and using a biocompatible polymer (PCL) as opposed to needing exotic materials or intricate moulds.

The sensor maintains measurable output across a broad pressure range, operating effectively up to 300 kPa. This exceeds the upper limits of many low-pressure sensors, such as those using natural leaf skeletons up to 60 kPa, air-gap structures up to 100 kPa, and aerogels up to 50 kPa. Although certain devices can function beyond 1 MPa, they typically exhibit significantly lower sensitivity in the low-pressure regime i.e., 10^{-3} –10^{-2} kPa^{-1}). From a fabrication standpoint, the device benefits from a low complexity and scalable process, relying solely on coaxial electrospinning and simple layer stacking without the need for lithography, moulding, or post treatments. In contrast, other high-performance designs frequently require additional steps such as UV curing, thermal imidization, or micro structuring. These factors collectively position the present sensor as a highly competitive candidate for next-generation flexible pressure sensors, particularly in applications requiring high sensitivity to subtle pressure variations with rapid response and manufacturability.

Table 3 shows comparison of fabrication process, materials used and other key parameters of hollow fiber flexible capacitive pressure sensor with flexible pressure sensors previously published in the literature.

Flexible sensors	Materials used (dielectric)	Sensitivity	Fabrication	Response time	Recovery time	Max. load	Ref.
Hollow nanofiber-based capacitive pressure sensor	PCL dielectric/ITO coated PET electrodes	1.05 kPa^{-1}	Electrospinning, simple fabrication and spray coating	84 ms	162 ms	300 kPa	This work
Plant-based biodegradable capacitive tactile pressure sensor	Leaf skeletons/flower petals/ AgNWs	0.08 kPa^{-1}	Simple fabrication and spray coating	-	-	60 kPa	[61]
Biodegradable rubber leaf skeleton based flexible pressure sensor	Leaf skeletons/ AgNWs	4.5×10^{-3} kPa^{-1}	Simple fabrication and spray coating	-	-	37 kPa	[62]
Flexible Capacitive Pressure Sensor with Cylindrical Ladder Microstructural Dielectric Layers	RG-067 electrically conductive silicone/PDMS	0.12 kPa^{-1}		21 ms	36 ms	204.7 kPa	[63]
Flexible Capacitive Pressure Sensor Based on a Cheetah Leg Structure via 3D Printing	PLA/ Poly(dimethylsiloxane) (Sylgard 184)	0.75 kPa^{-1}	Mold fabrication	80 ms		280 kPa	[64]
Flexible Capacitive Pressure Sensor Based on Alignment Airgap Dielectric	Indium Tin Oxide (ITO)/Polyethylene naphthalate (PEN)	1.277 kPa^{-1}	Mold fabrication	approx. 100 ms	approx. 100 ms	100 kPa	[65]

Graphene Aerogel-Based Pressure Sensors with Gradient Structure	Graphene aerogels	6.1 kPa^{-1}	freeze-assisted transfer printing strategy (FATPS)	50 ms	230 ms	50 kPa	[66]
Flexible Capacitive Pressure Sensor Based on a Porous Hollow Hemisphere Dielectric Layer	PDMS/PVA /CNT	0.18 kPa^{-1}	Simple fabrication and spray coating	52 ms	56 ms	50 kPa	[67]
Flexible capacitive pressure sensor based on strontium alginate with crater microstructure	flexible strontium alginate (SCA) films, PDMS, conductive cloth	-	Simple fabrication, spray coating	20 ms	50 ms	-	[68]
A wearable and high-performance capacitive pressure sensor based on a biocompatible PVP nanofiber membrane via electrospinning and UV treatment	Polyvinyl pyrrolidone (PVP) nanofibers/ PI film	0.278 kPa^{-1}	Electrospinning, UV treatment, and simple layer assembly fabrication	41 ms	36 ms	200 kPa	[69]
High-Performance Flexible Capacitive Pressure Sensor Based on a Spiked Nickel/Polyimide Composite Nanofiber Membrane	Nickel (Ni) particles, Polyimide (PI) electrospun nanofiber	4.04 MPa^{-1}	ELectrospinning, laser cutting, sensor packaging, ultrasonication	30 ms	40 ms	1.5 MPa	[70]
A flexible capacitive pressure sensor based on an electrospun polyimide nanofiber membrane	PI nanofiber, PI tape	2.204 kPa^{-1}	Electrospinning and mould	157.5 ms	175 ms	1.388 MPa	[71]

Flexible Capacitive Pressure Sensor Based on a Dual-Structured Nanofiber Membrane as the Dielectric	PI, conductive fabric, TPUNM dielectric	0.28 kPa^{-1}	Electrospinning	65 ms	78 ms	40 kPa	[72]
A new strategy for the fabrication of a flexible and highly sensitive capacitive pressure sensor	MXene/PVP	1.25 kPa^{-1}	Vacuum filtration, Laser irradiation	30 ms	15 ms	294 kPa	[73]
Flexible and Stretchable Capacitive Sensors with Different Microstructures	Glycerin/Chitosan & CuNWs	1.7 kPa^{-1}	Template method, spin-coating	180 ms	130 ms	1 MPa	[74]

4.8 Application Demonstration

To demonstrate the practical utility of the hollow nanofiber capacitive pressure sensor, a series of demonstrative tests in which the sensor was attached to the human body to function as an electronic skin (e-skin) for various applications. Figure 21 highlights several such demonstrations. In a tactile sensing scenario, the sensor was placed on the hand. When a light touch or tap was applied to the hand, distinct spikes in capacitance were recorded with each touch. The sensor could detect even gentle touches, with the signal magnitude corresponding to the pressure of the touch. This confirms that the device can serve as a touch or pressure pad, translating physical touch into electrical signals in real time. The response was instantaneous to each touch and returned to baseline after release, indicating good reversibility in practical application.

As a second example, the sensor was used for human motion detection. We mounted it over the radial artery area on the wrist (see Figure 21b), where it could experience slight bending and stretching during wrist movements. As the wrist is flexed and extended, the sensor produced clearly observable changes in capacitance that corresponded to the motion. Each wrist movement led to a characteristic waveform in the capacitance signal, demonstrating that the sensor can pick up subtle pressure/tension changes associated with joint motion. The signal was repeatable for consecutive movements, showing potential for use in activity monitoring or as a

wearable motion sensor. Consequently, the sensor's thin, flexible nature allowed it to conform to the skin and move with the body without hindrance. The ability to detect dynamic gestures like wrist flexion suggests that the hollow fiber sensor could be integrated into wearable systems for tracking body kinetics. For instance, as part of a smart sleeve or bracelet that monitors joint angles or muscle activity through pressure changes.

The most striking demonstration involved using the sensor to monitor vocal cord vibrations during speech. We attached the sensor to the throat (Figure 21c) and recorded the capacitance signal while the person was speaking and in rest. During normal speaking, the sensor detected periodic capacitance fluctuations that correspond to the vibrations of the vocal cords and the pressure waves from speech. When the person simply rested (not speaking), the capacitance remained relatively constant, but as soon as they began talking, oscillatory changes in relative capacitance can be seen. This indicates the sensor is sensitive enough to function as a throat microphone or voice activity monitor.

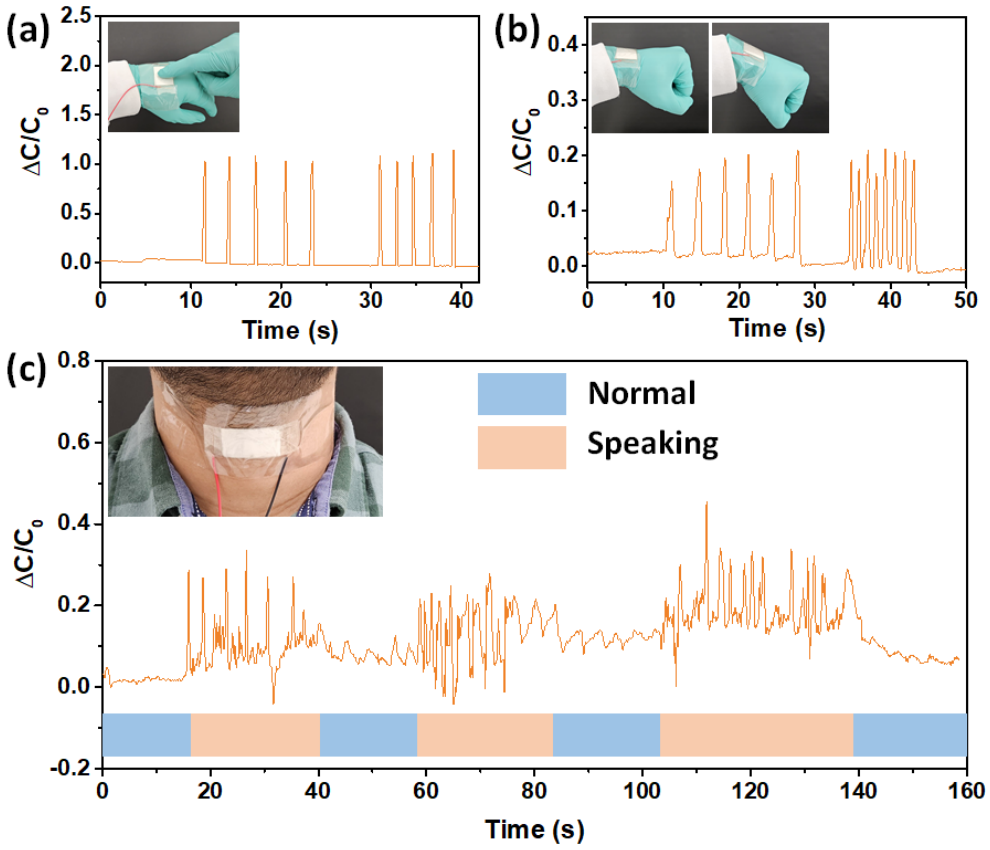

Figure 21 shows practical demonstration of flexible nanofiber sensor as an electronic skin. (a) shows touch sensing when mounted on hand. (b) shows joint movement sensing when mounted on wrist. (c) shows vocal cord vibrations when mounted on throat.

Furthermore, we compared the sensor output for speaking aloud and whispering. Speaking in a normal voice creates relatively large amplitude throat vibrations hence higher pressure on the

sensor, whereas whispering produces much subtler vibrations since the vocal cords move less and generate smaller pressure changes. Remarkably, our sensor was able to distinguish whispering from speaking. whispering results in a detectable but smaller amplitude signal i.e., 40dB, whereas speaking yielded a stronger signal i.e., 73dB as depicted in Figure 22. Even a very gentle, low-pressure oscillations from whispering were captured, underscoring the device high sensitivity to minute pressure variations. This demonstration suggests applications in voice recognition or vocal health monitoring. For instance, the sensor could be used in a wearable neck patch to continuously monitor speech patterns. The success in detecting whisper level pressures also validates that the performance of the sensor in the low-pressure regime translates to real biological signals, not just laboratory setups.

Collectively, these demonstrations highlight the versatility and effectiveness of the hollow fiber capacitive sensor as a wearable pressure sensing element. In all cases, the sensor showed a prompt and clear response, conforming to curved body surfaces without issue. The ability to capture both static and dynamic pressures, from the slight pressure of a whisper to the firmer pressure of a tap, showcases the wide operating range and sensitivity of our design. These results pave the way for potential medical and human-machine interface applications. For example, the sensor could be used for respiratory monitoring such as sensing chest movements or coughs or as intelligent bandages that respond to touch. It could also serve in soft robotics or prosthetics as an artificial skin that provides haptic feedback. The demonstration on the throat in particular points to use in voice prosthetics or silent speech interfaces where detecting vocal cord motion is crucial (addressing Speech Impairment). The combination of biodegradability and high performance makes it additionally attractive for transient or eco-friendly wearable devices. In conclusion, the real-world tests confirm that the hollow nanofiber sensor is not only a high performing device in the lab, but also practically applicable in scenarios requiring flexible skin mounted pressure sensing.

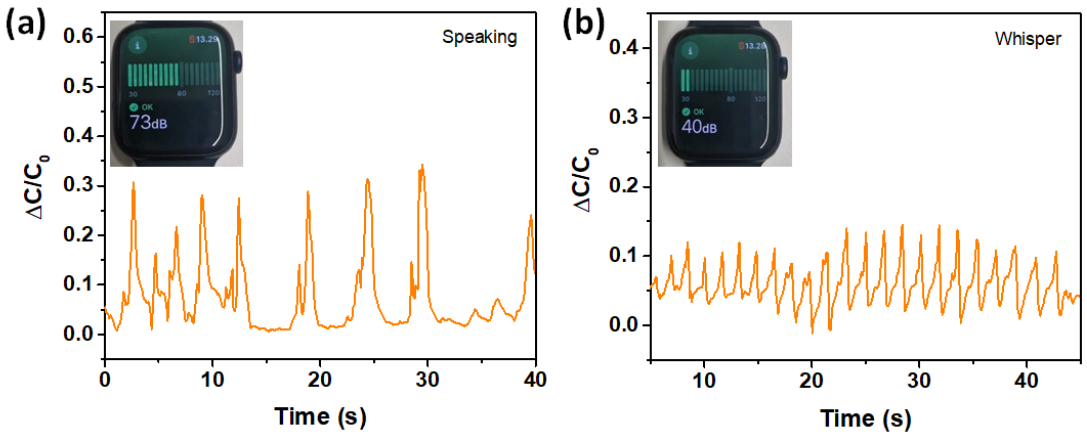

Figure 22 (a) shows detection of speaking vibrations of high frequency. (b) shows detecting whispering at subtle sound frequency.

5 Conclusion

This work has demonstrated that coaxially electrospun hollow PCL nanofibers can serve as highly effective dielectric layers for flexible capacitive pressure sensors. By employing a sacrificial core during electrospinning, we produced thin-walled hollow nanofibers that create a porous dielectric matrix filled with trapped air. The work also verifies models of porous dielectric behaviour. As pressure increases, the air pockets compress and eventually collapse, which produces nonlinear sensitivity across the pressure range consistent with predictions from dielectric composites theory. Experimentally, the sensors with hollow fiber dielectrics outperformed those with conventional solid-fiber dielectrics at low-pressure regime while maintaining a low detection limit. The response time of the hollow fiber sensors remained on the order of milliseconds, indicating that the micro- and nanoscale fiber network does not significantly slow down its electrical response. Moreover, cyclic testing showed excellent durability as it remained stable over thousands of compression cycles, demonstrating that the fibrous dielectric can withstand repeated loading without degradation. However, while the sensor demonstrated excellent sensitivity at lower pressures, a decrease in sensitivity was observed at higher pressures, where its performance fell below that of capacitive sensors based on single-shell electrospun fibers. This suggests the diminishing effect of hollow air gaps with increasing pressure. The coaxial electrospinning approach requires only common polymers and solvents, and avoids multi-step lamination or etching.

The enhanced performance of hollow fiber dielectrics suggests potential for improved tactile and wearable sensing applications, where detecting slight pressure changes is crucial. In particular, sensors based on this design could be integrated into electronic skin, soft robotics, or health-monitoring patches, leveraging both the mechanical compliance and biocompatibility of the materials. Future work can build on this foundation to optimize device architecture and explore applications ranging from touch interfaces to medical devices, where the unique combination of sensitivity, durability, and fabrication simplicity can be fully exploited.

6 Future Perspective

Despite these advances, several factors can be addressed for improvement and scale-up toward industrial application. Firstly, scalable fabrication and process automation are crucial. The coaxial electrospinning process can be enhanced by multi-nozzle or needle-less systems and real-time control. Adapting such high-throughput equipment to coaxial spinning (e.g., with parallel coaxial spinnerets) could exponentially increase production volume. Programmable syringe pumps and motorized stages would enable precise matching of core and shell flow rates, minimizing fiber defects and preventing shell collapse. Environmental controls i.e., temperature and humidity, around the spinneret and collector can stabilize the jet behaviour. For instance, consistent humidity prevents uneven solvent evaporation which reduces unstable spinning and jet clogging. In practice, a closed-loop system using real-time feedback (e.g., camera monitoring of jet shape or fiber diameter) could adjust parameters in-situ to maintain uniform hollow structures. These automation strategies would improve yield and reproducibility, moving the technology toward roll-to-roll or batch manufacturing.

Secondly, dielectric material engineering can further boost sensor performance. Embedding high-permittivity nanoparticles into the PCL matrix will raise the effective dielectric constant of the shell, increasing the baseline capacitance and sensitivity. As stated previously, adding ceramic nanoparticles like $BaTiO_3$ or alumina (Al_2O_3) into PDMS matrix has been shown to dramatically increase ε_r “yielded a substantial dielectric constant” and significantly enhanced sensor sensitivity [9]. A similar approach could be taken here by blending nano $BaTiO_3$ into the PCL solution prior to spinning. The concentration and dispersion of the particles should be optimized so as not to clog the spinneret or excessively stiffen the fiber. Another intriguing idea is to customize the core fluid by using a gas or highly volatile solvent as the core could produce hollow fibers with partially collapsed or textured inner cavities after spinning hence introducing additional micro-scale roughness and porosity. These hierarchical structures could amplify the compressibility even more.

A third direction is advanced manufacturing integration. Three-dimensional (3D) printing can be combined with the electrospun fibers to create complex sensor architectures. For instance, 3D printing can produce custom electrode patterns, spacers, or micro-lens structures that align with the nanofiber mat. He et al. recently demonstrated Digital Light Processing (DLP) 3D printing of nanostructured ion gels to make capacitive sensors with “superior sensing performances”. By analogy, one could 3D print a scaffold or frame (using UV-curable polymers

or elastomers) onto which the coaxial fibers are deposited, or into which the fiber mat is laminated. This would allow the sensor geometry such as pillar shape or edge structures, to be precisely controlled [75]. Another powerful concept is multi-layer stacking: layering multiple fiber mats separated by thin polymer films can multiply the overall capacitance and extend the dynamic range. A study reported a 12-layer stacked sensor achieving high initial capacitance and good stability [76]. In practice, one could stack alternating hollow and solid layers, or gradient-stiffness layers, to tailor the pressure–capacitance curve. Programmable 3D printers might even directly print gradient porosity or conductive ink onto the fiber surfaces to create integrated sensing arrays. These techniques would exploit the fiber dielectric flexibility while adding new degrees of freedom in design.

References

[1] P. G. Reddy *et al.*, "Biodegradable, Self-Adhesive, Stretchable, Transparent, and Versatile Electronic Skins Based on Intrinsically Hydrophilic Poly(Caproactone-Urethane) Elastomer," *Adv Eng Mater*, vol. 26, no. 24, p. 2401704, 2024, doi: https://doi.org/10.1002/adem.202401704.

[2] P. Guruprasad Reddy *et al.*, "Sustainable cross-linked poly(glycerol–co–δ–valerolactone) urethane substrates and multipurpose transparent electrodes for wearable electronics," *Chemical Engineering Journal*, vol. 495, p. 153531, 2024, doi: https://doi.org/10.1016/j.cej.2024.153531.

[3] A. Elsayes, V. Sharma, K. Yiannacou, A. Koivikko, A. Rasheed, and V. Sariola, "Plant-Based Biodegradable Capacitive Tactile Pressure Sensor Using Flexible and Transparent Leaf Skeletons as Electrodes and Flower Petal as Dielectric Layer," *Adv Sustain Syst*, vol. 4, no. 9, p. 2000056, 2020, doi: https://doi.org/10.1002/adsu.202000056.

[4] X. Qu *et al.*, "Highly Sensitive Fiber Pressure Sensors over a Wide Pressure Range Enabled by Resistive-Capacitive Hybrid Response," *ACS Nano*, vol. 17, no. 15, pp. 14904–14915, Aug. 2023, doi: 10.1021/acsnano.3c03484.

[5] A. E. Fetz, C. A. Fantaziu, R. A. Smith, M. Z. Radic, and G. L. Bowlin, "Surface Area to Volume Ratio of Electrospun Polydioxanone Templates Regulates the Adsorption of Soluble Proteins from Human Serum," *Bioengineering*, vol. 6, no. 3, 2019, doi: 10.3390/bioengineering6030078.

[6] N. Asano, S. Sugihara, S. Suye, and S. Fujita, "Electrospun Porous Nanofibers with Imprinted Patterns Induced by Phase Separation of Immiscible Polymer Blends," *ACS Omega*, vol. 7, no. 23, pp. 19997–20005, Jun. 2022, doi: 10.1021/acsomega.2c01798.

[7] N. Shao, J. Wu, X. Yang, J. Yao, Y. Shi, and Z. Zhou, "Flexible capacitive pressure sensor based on multi-walled carbon nanotube electrodes," *Micro Nano Lett*, vol. 12, no. 1, pp. 45–48, Jan. 2017, doi: https://doi.org/10.1049/mnl.2016.0529.

[8] J. Qin *et al.*, "Flexible and Stretchable Capacitive Sensors with Different Microstructures," *Advanced Materials*, vol. 33, no. 34, p. 2008267, Aug. 2021, doi: https://doi.org/10.1002/adma.202008267.

[9] J. Li *et al.*, "Flexible BaTiO3-PDMS Capacitive Pressure Sensor of High Sensitivity with Gradient Micro-Structure by Laser Engraving and Molding," *Polymers (Basel)*, vol. 15, no. 15, Aug. 2023, doi: 10.3390/polym15153292.

[10] P. Rathore and J. D. Schiffman, "Beyond the Single-Nozzle: Coaxial Electrospinning Enables Innovative Nanofiber Chemistries, Geometries, and Applications," *ACS Appl Mater Interfaces*, vol. 13, no. 1, pp. 48–66, Jan. 2021, doi: 10.1021/acsami.0c17706.

[11] H. Yuan *et al.*, “Progress and challenges in flexible capacitive pressure sensors: Microstructure designs and applications,” *Chemical Engineering Journal*, vol. 485, p. 149926, 2024, doi: https://doi.org/10.1016/j.cej.2024.149926.

[12] Z. Zheng, Y. Pan, and H. Huang, “A Capacitive Pressure Sensor with a Hierarchical Microporous Scaffold Prepared by Melt Near-Field Electro-Writing,” *Sensors*, vol. 25, no. 9, 2025, doi: 10.3390/s25092814.

[13] K. Keshyagol, S. Hiremath, V. H. M., P. K. Rao, P. Hiremath, and N. Naik, “Analysis of Polymer-Ceramic Composites Performance on Electrical and Mechanical Properties through Finite Element and Empirical Models,” *Materials*, vol. 17, no. 15, 2024, doi: 10.3390/ma17153837.

[14] “Capacitive Sensor Market - By Type (Touch Sensors, Motion Sensors, Position Sensors, Proximity Sensors, Level Sensors, Humidity Sensors, Pressure Sensors, Temperature Sensors, Force Sensors, Accelerometers, Flow Sensors), By Technology, By Application & Forecast, 2024 – 2032,” Aug. 2024.

[15] M. A. Haghighat Bayan, F. Afshar Taromi, M. Lanzi, and F. Pierini, “Enhanced efficiency in hollow core electrospun nanofiber-based organic solar cells,” *Sci Rep*, vol. 11, no. 1, p. 21144, 2021, doi: 10.1038/s41598-021-00580-4.

[16] R. Qin *et al.*, “A new strategy for the fabrication of a flexible and highly sensitive capacitive pressure sensor,” *Microsyst Nanoeng*, vol. 7, no. 1, p. 100, 2021, doi: 10.1038/s41378-021-00327-1.

[17] T. Hua *et al.*, “A Sensitivity-Optimized Flexible Capacitive Pressure Sensor with Cylindrical Ladder Microstructural Dielectric Layers,” *Sensors*, vol. 23, no. 9, 2023, doi: 10.3390/s23094323.

[18] Y. Zhang, R. Howver, B. Gogoi, and N. Yazdi, “A high-sensitive ultra-thin MEMS capacitive pressure sensor,” in *2011 16th International Solid-State Sensors, Actuators and Microsystems Conference*, 2011, pp. 112–115. doi: 10.1109/TRANSDUCERS.2011.5969151.

[19] M. Ren *et al.*, “A wearable and high-performance capacitive pressure sensor based on a biocompatible PVP nanofiber membrane via electrospinning and UV treatment,” *J. Mater. Chem. C*, vol. 10, no. 29, pp. 10491–10499, 2022, doi: 10.1039/D2TC00955B.

[20] M. Ahmadi Bonakdar and D. Rodrigue, “Electrospinning: Processes, Structures, and Materials,” Mar. 01, 2024, *Multidisciplinary Digital Publishing Institute (MDPI)*. doi: 10.3390/macromol4010004.

[21] J. H. Yu, S. Fridrikh, and G. C. Rutledge, “Production of Submicrometer Diameter Fibers by Two-Fluid Electrospinning,” *Advanced Materials*, vol. 16, pp. 1562–1566, Aug. 2004, doi: 10.1002/adma.200306644.

[22] D. Li, A. Babel, S. A. Jenekhe, and Y. N. Xia, “Nanofibers of Conjugated Polymers Prepared by Electrospinning with a Two-Capillary Spinneret,” *Advanced Materials*, vol. 16, pp. 2062–2066, Nov. 2004, doi: 10.1002/adma.200400606.

[23] A. K. Moghe and B. S. and Gupta, “Co-axial Electrospinning for Nanofiber Structures: Preparation and Applications,” *Polymer Reviews*, vol. 48, no. 2, pp. 353–377, May 2008, doi: 10.1080/15583720802022257.

[24] Z. Sun, E. Zussman, A. L. Yarin, J. H. Wendorff, and A. Greiner, “Compound Core–Shell Polymer Nanofibers by Co-Electrospinning,” *Advanced Materials*, vol. 15, no. 22, pp. 1929–1932, Nov. 2003, doi: https://doi.org/10.1002/adma.200305136.

[25] D. Li, J. T. McCann, and Y. Xia, “Use of Electrospinning to Directly Fabricate Hollow Nanofibers with Functionalized Inner and Outer Surfaces,” *Small*, vol. 1, no. 1, pp. 83–86, Jan. 2005, doi: https://doi.org/10.1002/smll.200400056.

[26] L. Larrondo and R. St. John Manley, “Electrostatic fiber spinning from polymer melts. I. Experimental observations on fiber formation and properties,” *Journal of Polymer Science: Polymer Physics Edition*, vol. 19, no. 6, pp. 909–920, Jun. 1981, doi: https://doi.org/10.1002/pol.1981.180190601.

[27] J. Choi, J. Lee, J. Choi, D. Jung, and S. E. Shim, “Electrospun PEDOT:PSS/PVP nanofibers as the chemiresistor in chemical vapour sensing,” *Synth Met*, vol. 160, no. 13, pp. 1415–1421, 2010, doi: https://doi.org/10.1016/j.synthmet.2010.04.021.

[28] A. K. Moghe and B. S. Gupta, “Co-axial electrospinning for nanofiber structures: Preparation and applications,” *Polymer Reviews*, vol. 48, no. 2, pp. 353–377, Apr. 2008, doi: 10.1080/15583720802022257.

[29] D. Li and Y. Xia, “Direct Fabrication of Composite and Ceramic Hollow Nanofibers by Electrospinning,” *Nano Lett*, vol. 4, no. 5, pp. 933–938, May 2004, doi: 10.1021/nl049590f.

[30] Z.-C. Yao, M.-W. Chang, Z. Ahmad, and J.-S. Li, “Encapsulation of rose hip seed oil into fibrous zein films for ambient and on demand food preservation via coaxial electrospinning,” *J Food Eng*, vol. 191, pp. 115–123, 2016, doi: https://doi.org/10.1016/j.jfoodeng.2016.07.012.

[31] J. H. Yu, S. Fridrikh, and G. C. Rutledge, “Production of Submicrometer Diameter Fibers by Two-Fluid Electrospinning,” *Advanced Materials*, vol. 16, pp. 1562–1566, Aug. 2004, doi: 10.1002/adma.200306644.

[32] J. Di *et al.*, “Fabrication of Zeolite Hollow Fibers by Coaxial Electrospinning,” *Chemistry of Materials*, vol. 20, no. 11, pp. 3543–3545, Jun. 2008, doi: 10.1021/cm8006809.

[33] T. Song, Y. Z. Zhang, and T. J. Zhou, “Fabrication of magnetic composite nanofibers of poly(ε-caprolactone) with FePt nanoparticles by coaxial electrospinning,” *J Magn Magn*

Mater, vol. 303, no. 2, pp. e286–e289, 2006, doi: https://doi.org/10.1016/j.jmmm.2006.01.247.

[34] C. J. Luo and M. Edirisinghe, "Core-Liquid-Induced Transition from Coaxial Electrospray to Electrospinning of Low-Viscosity Poly(lactide-co-glycolide) Sheath Solution," *Macromolecules*, vol. 47, no. 22, pp. 7930–7938, Nov. 2014, doi: 10.1021/ma5016616.

[35] I. G. Loscertales, A. Barrero, I. Guerrero, R. Cortijo, M. Marquez, and A. M. Gañán-Calvo, "Micro/Nano Encapsulation via Electrified Coaxial Liquid Jets," *Science (1979)*, vol. 295, no. 5560, pp. 1695–1698, Mar. 2002, doi: 10.1126/science.1067595.

[36] R. Nayak, R. Padhye, and L. Arnold, "2 - Melt-electrospinning of nanofibers," in *Electrospun Nanofibers*, M. Afshari, Ed., Woodhead Publishing, 2017, pp. 11–40. doi: https://doi.org/10.1016/B978-0-08-100907-9.00002-7.

[37] S. Mathew and K. Chintagumpala, "Design and characterization of PDMS-CB-ZnO-ternary composite based flexible capacitance pressure sensors for wearable applications," *Flexible and Printed Electronics*, vol. 10, no. 2, p. 25004, Apr. 2025, doi: 10.1088/2058-8585/adc81e.

[38] M. Chen *et al.*, "Touchpoint-Tailored Ultrasensitive Piezoresistive Pressure Sensors with a Broad Dynamic Response Range and Low Detection Limit," *ACS Appl Mater Interfaces*, vol. 11, no. 2, pp. 2551–2558, Jan. 2019, doi: 10.1021/acsami.8b20284.

[39] Y. Wan *et al.*, "A Highly Sensitive Flexible Capacitive Tactile Sensor with Sparse and High-Aspect-Ratio Microstructures," *Adv Electron Mater*, vol. 4, no. 4, p. 1700586, Apr. 2018, doi: https://doi.org/10.1002/aelm.201700586.

[40] Y. Zhao *et al.*, "Highly Sensitive and Flexible Capacitive Pressure Sensors Combined with Porous Structure and Hole Array Using Sacrificial Templates and Laser Ablation," *Polymers (Basel)*, vol. 16, no. 16, Aug. 2024, doi: 10.3390/polym16162369.

[41] Z. Guo *et al.*, "Printed and flexible capacitive pressure sensor with carbon nanotubes based composite dielectric layer," *Micromachines (Basel)*, vol. 10, no. 11, Nov. 2019, doi: 10.3390/mi10110715.

[42] Y. Zhu *et al.*, "A flexible capacitive pressure sensor based on an electrospun polyimide nanofiber membrane," *Org Electron*, vol. 84, p. 105759, 2020, doi: https://doi.org/10.1016/j.orgel.2020.105759.

[43] J. Wang, Y. Lou, B. Wang, Q. Sun, M. Zhou, and X. Li, "Highly sensitive, breathable, and flexible pressure sensor based on electrospun membrane with assistance of AgNW/TPU as composite dielectric layer," *Sensors (Switzerland)*, vol. 20, no. 9, May 2020, doi: 10.3390/s20092459.

[44] S. Siddique, A. Barua, R. Gogoi, and V. Sharma, "Electrospun Hollow Nanofiber Surfaces as Dielectric Mediums for Highly Sensitive Flexible Capacitive Pressure

Sensors in Low-Pressure Regimes," *IEEE Journal on Flexible Electronics*, p. 1, 2025, doi: 10.1109/JFLEX.2025.3577111.

[45] X. Qu *et al.*, "Highly Sensitive Fiber Pressure Sensors over a Wide Pressure Range Enabled by Resistive-Capacitive Hybrid Response," *ACS Nano*, vol. 17, no. 15, pp. 14904–14915, Aug. 2023, doi: 10.1021/acsnano.3c03484.

[46] J. Wang, Y. Lou, B. Wang, Q. Sun, M. Zhou, and X. Li, "Highly Sensitive, Breathable, and Flexible Pressure Sensor Based on Electrospun Membrane with Assistance of AgNW/TPU as Composite Dielectric Layer," *Sensors*, vol. 20, no. 9, 2020, doi: 10.3390/s20092459.

[47] Y. Wu *et al.*, "A stretchable all-nanofiber iontronic pressure sensor," *Soft Science*, vol. 3, no. 4, 2023, doi: 10.20517/ss.2023.24.

[48] X. Yang, Y. Wang, and X. Qing, "Electrospun Ionic Nanofiber Membrane-Based Fast and Highly Sensitive Capacitive Pressure Sensor," *IEEE Access*, vol. 7, pp. 139984–139993, 2019, doi: 10.1109/ACCESS.2019.2943736.

[49] J. Xu *et al.*, "High sensitivity and broad linearity range pressure sensor based on hierarchical in-situ filling porous structure," *npj Flexible Electronics*, vol. 6, no. 1, p. 62, 2022, doi: 10.1038/s41528-022-00191-7.

[50] Y. Zhu, W. Lu, Y. Guo, Y. Chen, Y. Wu, and H. Lu, "Biocompatible, stretchable and mineral PVA–gelatin–nHAP hydrogel for highly sensitive pressure sensors," *RSC Adv.*, vol. 8, no. 65, pp. 36999–37007, 2018, doi: 10.1039/C8RA06193A.

[51] Q. Zhang *et al.*, "Hierarchically structured hollow PVDF nanofibers for flexible piezoelectric sensor," *Chemical Engineering Journal*, vol. 498, p. 155661, 2024, doi: https://doi.org/10.1016/j.cej.2024.155661.

[52] X. Qu *et al.*, "Highly Sensitive Capacitive Fiber Pressure Sensors Enabled by Electrode and Dielectric Layer Regulation," *ACS Appl Mater Interfaces*, vol. 15, no. 47, pp. 54966–54976, Nov. 2023, doi: 10.1021/acsami.3c13714.

[53] P. C. Uzabakiriho, M. Wang, C. Ma, and G. Zhao, "Stretchable, breathable, and highly sensitive capacitive and self-powered electronic skin based on core–shell nanofibers," *Nanoscale*, vol. 14, no. 17, pp. 6600–6611, 2022, doi: 10.1039/D2NR00444E.

[54] Z. Shao, X. Zhang, Z. Song, J. Liu, X. Liu, and C. Zhang, "Simulation Guided Coaxial Electrospinning of Polyvinylidene Fluoride Hollow Fibers with Tailored Piezoelectric Performance," *Small*, vol. 19, no. 38, p. 2303285, 2023, doi: https://doi.org/10.1002/smll.202303285.

[55] M. Suzuki, Y. Tachibana, and K. Kasuya, "Biodegradability of poly(3-hydroxyalkanoate) and poly(ε-caprolactone) via biological carbon cycles in marine environments," *Polym J*, vol. 53, no. 1, pp. 47–66, 2021, doi: 10.1038/s41428-020-00396-5.

[56] N. Kumar Kalita, D. Hazarika, R. K. Srivastava, and M. Hakkarainen, “Faster biodegradable and chemically recyclable polycaprolactone with embedded enzymes: Revealing new insights into degradation kinetics,” *Chemical Engineering Journal*, vol. 496, p. 153982, 2024, doi: https://doi.org/10.1016/j.cej.2024.153982.

[57] X. He *et al.*, “Microstructured capacitive sensor with broad detection range and long-term stability for human activity detection,” *npj Flexible Electronics*, vol. 5, no. 1, p. 17, 2021, doi: 10.1038/s41528-021-00114-y.

[58] M. O. G. Nayeem *et al.*, “All-nanofiber–based, ultrasensitive, gas-permeable mechanoacoustic sensors for continuous long-term heart monitoring,” *Proceedings of the National Academy of Sciences*, vol. 117, no. 13, pp. 7063–7070, Mar. 2020, doi: 10.1073/pnas.1920911117.

[59] J. Zhou *et al.*, “Electrospun biosensors for biomarker detection,” *Colloid Interface Sci Commun*, vol. 59, p. 100767, 2024, doi: https://doi.org/10.1016/j.colcom.2024.100767.

[60] J. Liu *et al.*, “Graphene Aerogel-Based Pressure Sensors with Gradient Structure for Subtle Physiological Signals and Motion Monitoring,” *Adv Mater Technol*, vol. 9, no. 10, p. 2302169, May 2024, doi: https://doi.org/10.1002/admt.202302169.

[61] A. Elsayes *et al.*, “Plant-Based Biodegradable Capacitive Tactile Pressure Sensor Using Flexible and Transparent Leaf Skeletons as Electrodes and Flower Petal as Dielectric Layer,” *Adv Sustain Syst*, vol. 4, no. 9, p. 2000056, Sep. 2020, doi: 10.1002/ADSU.202000056.

[62] A. Koivikko, V. Sharma, V. Lampinen, K. Yiannacou, and V. Sariola, “Biodegradable, Flexible and Transparent Tactile Pressure Sensor Based on Rubber Leaf Skeletons,” *Proceedings of IEEE Sensors*, vol. 2020-October, Oct. 2020, doi: 10.1109/SENSORS47125.2020.9278756.

[63] T. Hua *et al.*, “A Sensitivity-Optimized Flexible Capacitive Pressure Sensor with Cylindrical Ladder Microstructural Dielectric Layers,” *Sensors*, vol. 23, no. 9, p. 4323, May 2023, doi: 10.3390/S23094323/S1.

[64] W. Hong *et al.*, “Flexible Capacitive Pressure Sensor with High Sensitivity and Wide Range Based on a Cheetah Leg Structure via 3D Printing,” *ACS Appl Mater Interfaces*, vol. 15, no. 39, pp. 46347–46356, Oct. 2023, doi: 10.1021/ACSAMI.3C09841/ASSET/IMAGES/LARGE/AM3C09841_0009.JPEG.

[65] S. W. Kim *et al.*, “A Highly Sensitive and Flexible Capacitive Pressure Sensor Based on Alignment Airgap Dielectric,” *Sensors*, vol. 22, no. 19, p. 7390, Oct. 2022, doi: 10.3390/S22197390/S1.

[66] J. Liu *et al.*, “Graphene Aerogel-Based Pressure Sensors with Gradient Structure for Subtle Physiological Signals and Motion Monitoring,” *Adv Mater Technol*, vol. 9, no. 10, p. 2302169, May 2024, doi: 10.1002/ADMT.202302169.

[67] H. Cui *et al.*, “A Sensitive and Flexible Capacitive Pressure Sensor Based on a Porous Hollow Hemisphere Dielectric Layer,” *Micromachines 2023, Vol. 14, Page 662*, vol. 14, no. 3, p. 662, Mar. 2023, doi: 10.3390/MI14030662.

[68] M. Xu *et al.*, “A highly sensitive, flexible capacitive pressure sensor based on strontium alginate with crater microstructure,” *J Alloys Compd*, vol. 997, p. 174904, Aug. 2024, doi: 10.1016/J.JALLCOM.2024.174904.

[69] M. Ren *et al.*, “A wearable and high-performance capacitive pressure sensor based on a biocompatible PVP nanofiber membrane via electrospinning and UV treatment,” *J Mater Chem C Mater*, vol. 10, no. 29, pp. 10491–10499, Jul. 2022, doi: 10.1039/D2TC00955B.

[70] L. Xia *et al.*, “High-Performance Flexible Capacitive Pressure Sensor Based on a Spiked Nickel/Polyimide Composite Nanofiber Membrane,” *ACS Sens*, vol. 10, p. 45, 2025, doi: 10.1021/ACSSENSORS.4C03495/ASSET/IMAGES/LARGE/SE4C03495_0008.JPEG.

[71] Y. Zhu *et al.*, “A flexible capacitive pressure sensor based on an electrospun polyimide nanofiber membrane,” *Org Electron*, vol. 84, p. 105759, Sep. 2020, doi: 10.1016/J.ORGEL.2020.105759.

[72] R. Li, M. Panahi-Sarmad, T. Chen, A. Wang, R. Xu, and X. Xiao, “Highly Sensitive and Flexible Capacitive Pressure Sensor Based on a Dual-Structured Nanofiber Membrane as the Dielectric for Attachable Wearable Electronics,” *ACS Appl Electron Mater*, vol. 4, no. 1, pp. 469–477, Jan. 2022, doi: 10.1021/ACSAELM.1C01098/ASSET/IMAGES/LARGE/EL1C01098_0007.JPEG.

[73] R. Qin *et al.*, “A new strategy for the fabrication of a flexible and highly sensitive capacitive pressure sensor,” *Microsystems & Nanoengineering 2021 7:1*, vol. 7, no. 1, pp. 1–12, Nov. 2021, doi: 10.1038/s41378-021-00327-1.

[74] Z. Song *et al.*, “Biodegradable and flexible capacitive pressure sensor for electronic skins,” *Org Electron*, vol. 106, p. 106539, Jul. 2022, doi: 10.1016/J.ORGEL.2022.106539.

[75] X. He *et al.*, “Highly conductive and stretchable nanostructured ionogels for 3D printing capacitive sensors with superior performance,” *Nat Commun*, vol. 15, no. 1, p. 6431, 2024, doi: 10.1038/s41467-024-50797-w.

[76] Y. Zhu *et al.*, “A new strategy for fabricating a stacked flexible capacitive sensor,” *Functional Composite Materials*, vol. 5, no. 1, p. 9, 2024, doi: 10.1186/s42252-024-00058-2.

Appendices

Sensitivity Test

Sensitivity tests is programmed based on a MATLAB script. The MATLAB is interfaced with LCR meter which is electrically connected to the sensor mounted on the TA. The MATLAB script run for specific pressures and gave output in the form of capacitance.

Matlab Script (Presented in its original form without any formatting)

```
s = [];
s = serialport("COM5", 9600);
configureTerminator(s, "LF")

writeline(s, 'FUNC csrs')
writeline(s, 'FUNC?')

%try
 %   assert(readline(s) == 'csrs');
%catch
  %  disp('Unexpected response from LCR meter');
    % Add code to handle the unexpected response here
    % For example, you can decide to exit the loop or take appropriate action
 %   break;
%end

writeline(s, 'FUNC:IMP:RANG:AUTO ON')
writeline(s, 'FREQ 1KHZ')
writeline(s, 'APER FAST')
writeline(s, 'CORR:OPEN:STAT 0')
writeline(s, 'TRIG:SOUR BUS')
writeline(s, 'COMP OFF')

tic;
data = [];

% Initialize min and max values
%minY = inf;
%maxY = -inf;

while (true)
    %writeline(s, 'TRIG');
    %writeline(s, 'FETC?');
    datastr = readline(s);
    values = sscanf(datastr, '%f,%f');

    if numel(values) == 2
        elapsedTime = toc;
        data = [data; [elapsedTime, values']];

        % Update min and max values
 %       minY = min(minY, min(data(:, 2)));
  %      maxY = max(maxY, max(data(:, 2)));
```

```
        %Capacitance
        plot(data(:, 1), data(:, 2));
        %demo+
        %plot(data(:, 1), data(:, 2), 'Linewidth',4);

        %Resistance
        %plot(data(:, 1), smooth(data(:, 3), 3),'Linewidth',4);
        %plot(data(:, 1), data(:, 3));
        %plot(data(:, 1), smooth(data(:, 3), 3));



        % Only set the y-axis limits if minY and maxY are valid
   %     if minY < maxY
    %        ylim([minY, maxY]);
     %   end

        %xlim([0, max(data(:, 1))]);
    end
end

%writeline(s, 'TRIG:SOUR INT');
s = [];
```

Exponent Connect Parameters

TA is integrated with the software named, “Exponent Connect” Each type of testing analysis has its TA Settings. Figure 23 shows parameters for sensitivity analysis at 1kPa.

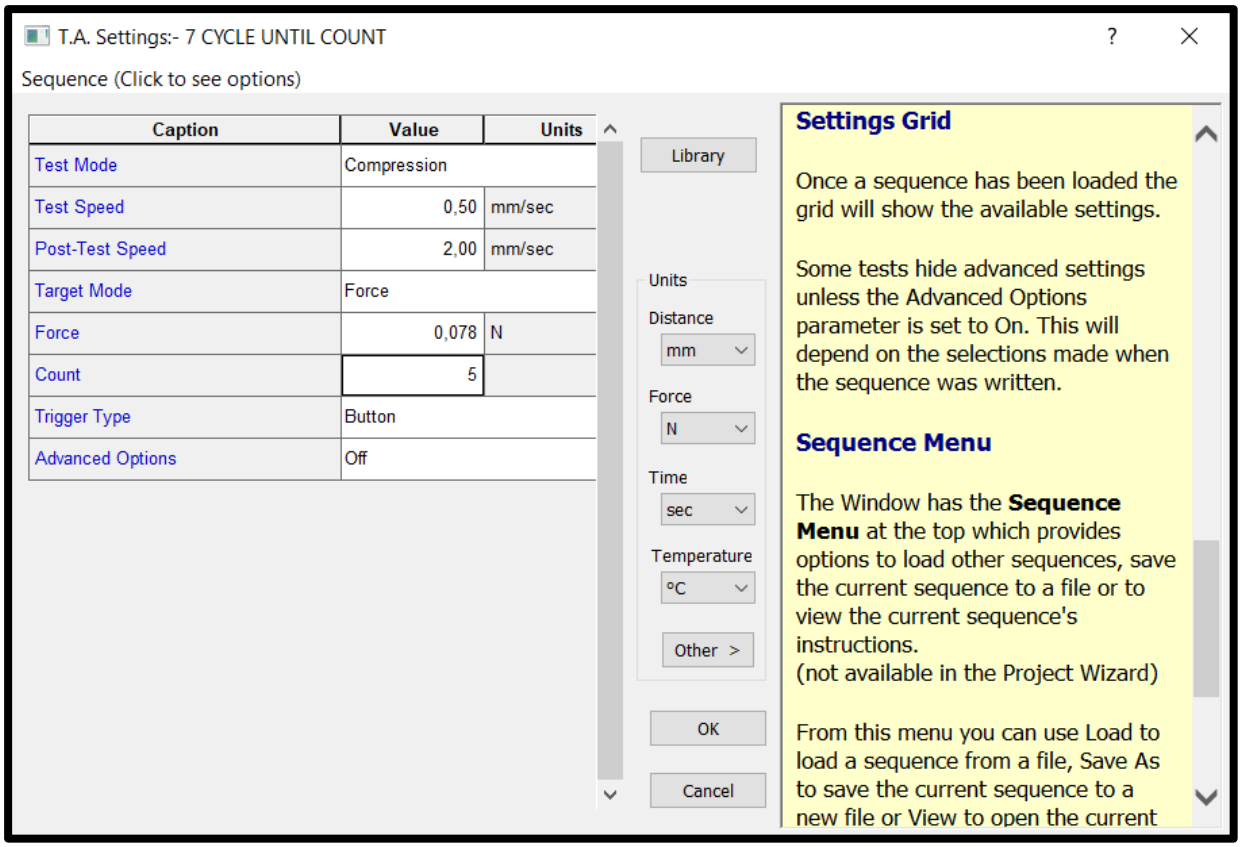

Figure 23 shows TA Parameters for Sensitivity Analysis at 1 kPa.

Cyclic Testing

The capacitive sensor is characterised for 1000 cycles demonstrating its durability. Cyclic testing is programmed based on a MATLAB script which is shown below;

Matlab Script (Presented in its original form without any formatting)

```
s = [];
s = serialport("COM5", 9600);
configureTerminator(s, "LF")

writeline(s, 'FUNC csrs')
writeline(s, 'FUNC?')

writeline(s, 'FUNC:IMP:RANG:AUTO ON')
writeline(s, 'FREQ 1KHZ')
writeline(s, 'APER FAST')
writeline(s, 'CORR:OPEN:STAT 0')
writeline(s, 'TRIG:SOUR BUS')
writeline(s, 'COMP OFF')

% === SET THIS based on your setup ===
cycle_duration = 20; % seconds per cycle — change based on your test setup
num_cycles = 1000;
```

```
target_time = num_cycles * cycle_duration;

tic;
data = [];

while true
    datastr = readline(s);
    values = sscanf(datastr, '%f,%f');

    if numel(values) == 2
        elapsedTime = toc;
        data = [data; [elapsedTime, values']];

        % Plot capacitance vs time
        plot(data(:, 1), data(:, 2));
        xlabel('Time (s)');
        ylabel('Capacitance');
        title('Capacitance vs Time');
        drawnow;

        % === Stop condition ===
        if elapsedTime >= target_time
            disp('Test complete: 1000 cycles reached.');
            break;
        end
    end
end

s = [];
```

Exponent Connect Parameters

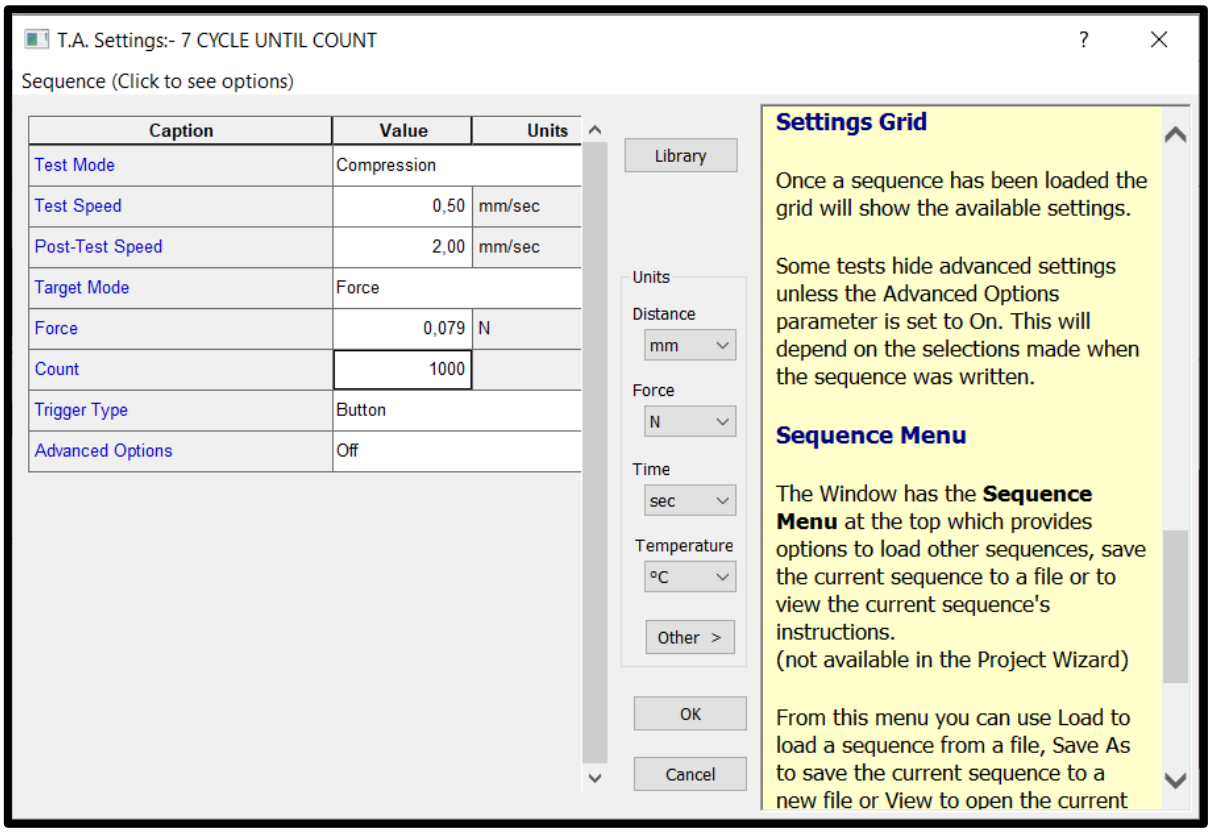

Figure 24 shows TA parameters of Cyclic Testing.

Stepwise Response Time

The parameters for stepwise response time are shown in Figure 25;

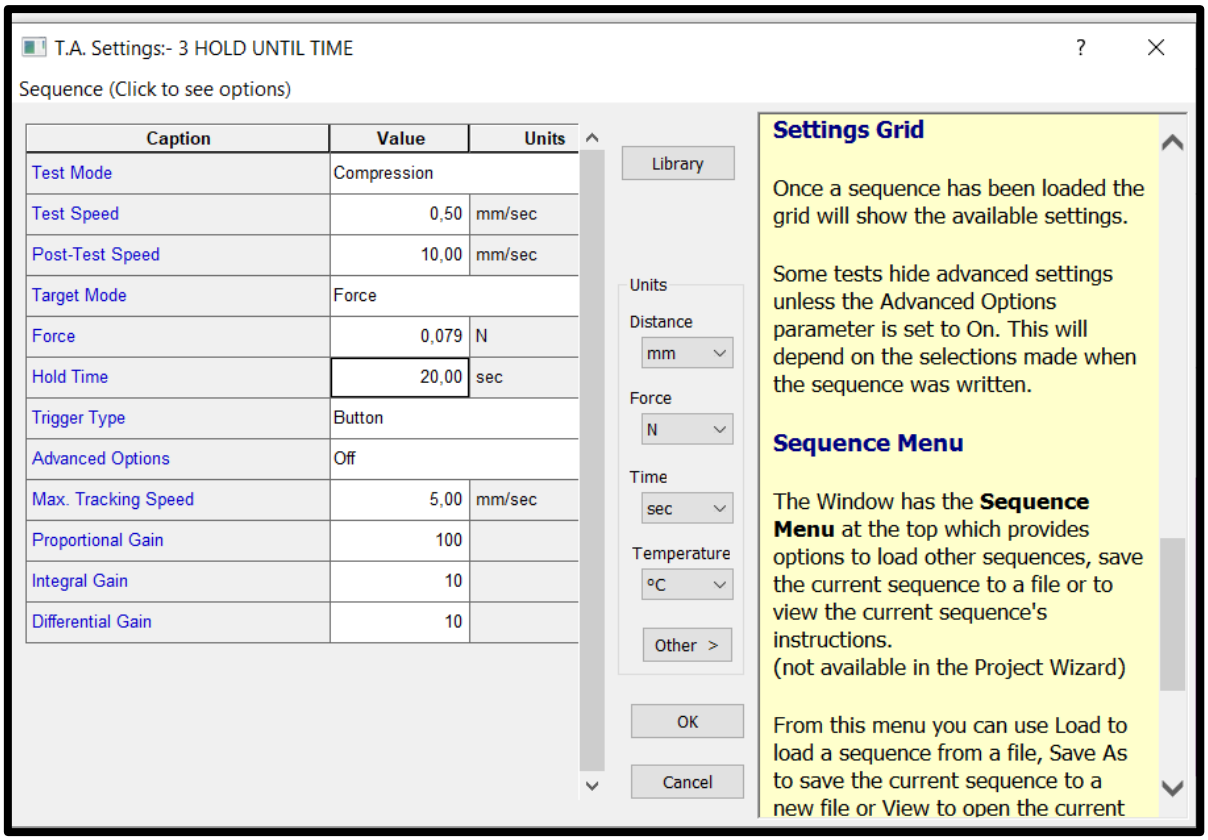

Figure 25 shows stepwise response time of the sensor at 1 kPa.